Mechanical Systems and Signal Processing 217 (2024) 111538

Contents lists available at ScienceDirect

Mechanical Systems and Signal Processing

journal homepage: www.elsevier.com/locate/ymssp

Corrosion damage identification based on the symmetry of propagating wavefield measured by a circular array of piezoelectric transducers: Theoretical, experimental and numerical studies

Beata Zima [a,*], Jochen Moll [b,c]

[a] Faculty of Mechanical Engineering and Ship Technology, Gdańsk University of Technology, 80-233 Gdańsk, Poland
[b] Department of Physics, Goethe University Frankfurt, 60438 Frankfurt, Germany
[c] Department of Mechanical Engineering, University of Siegen, 57076 Siegen, Germany

ARTICLE INFO

Communicated by Steffen Marburg

Keywords:
Guided waves
Irregular plate
Numerical simulations
Random fields
Experimental tests
Innovative systems

ABSTRACT

The article investigates the results obtained from numerical simulations and experimental tests concerning the propagation of guided waves in corroded steel plates. Developing innovative methodologies for assessing corrosion-induced degradation is crucial for accurately diagnosing offshore and ship structures exposed to harsh environmental conditions. The main aim of the research is to analyze how surface irregularities affect wave propagation characteristics. An investigation was conducted for antisymmetric fundamental mode A0. Specifically, the study examines the asymmetrical wavefronts generated by nonuniform thickness in damaged specimens. Initially, numerical analysis explores the impact of thickness variation on wave field symmetry. Corroded plates with varying levels of degradation are modeled using the random fields approach, with degradation levels ranging from 0 % to 60 %. Subsequently, the research investigates how the standard deviation of thickness distribution (from 5 % to 20 % of the initial thickness) and excitation frequency (from 50 to 150 kHz) influence recorded signals and the shape of reconstructed wavefronts. Each scenario compares wavefront symmetry levels estimated using rotational and bilateral symmetry degrees as indicative parameters. The numerical simulations are complemented by experimental tests conducted on plates with three different degradation levels. The results demonstrate the efficacy of the proposed wave field analysis approach for assessing structural integrity, as evidenced by the agreement between numerical predictions and experimental observations.

1. Introduction

Corrosion is one of the most prevalent forms of degradation observed in metallic structures [1–3]. Its accurate quantification is paramount, particularly in structures that endure constant exposure to harsh environmental conditions, such as marine vessels and offshore installations. The conventional nondestructive methodology, based on ultrasonic testing, as recommended by Classification Societies [4], presents several noteworthy limitations. It necessitates the application of a coupling agent, which can potentially

* Corresponding author.
E-mail address: beata.zima@pg.edu.pl (B. Zima).

https://doi.org/10.1016/j.ymssp.2024.111538
Received 23 February 2024; Received in revised form 10 May 2024; Accepted 15 May 2024
Available online 19 May 2024

influence the integrity of the structure under examination [5,6]. Although ultrasonic measurements facilitate the generation of thickness maps, their precision is inherently contingent upon the density and distribution of measurement points, given that ultrasonic transducers offer information concerning thickness at a single point during any given measurement. Additionally, this inspection method can be insufficient for localized damages caused by pitting corrosion. Guided wave propagation offers the possibility for both thickness reduction assessment and detection and localization of localized pits and cracks.

One of the most critical advantages of Lamb waves is their possibility to travel relatively long distances without significant amplitude reduction [7]. Their dispersive capabilities have been successfully used for general corrosion assessment. It can be defined as the attack of the entire metal surface exposed to the corrosive environment, resulting in uniform metal loss from the exposed surface. Because the specimen thickness determines the velocity of the guided wave, the thickness reduction entails changes in propagation velocity. This assumption is the base of many developed wave-based diagnostics methods dedicated to general corrosion assessment. Farhidzadeh and Salamone [8] used dispersion curves, continuous wavelet transform, and wave velocity measurement to quantify corrosion damage and diameter reduction of multiwire prestressing steel strands. The thickness reduction of ship structural elements has been estimated by Zima et al. [9] using guided waves and spectral decomposition. The corrosion imaging algorithm based on the Riesz transform to identify corrosion on metal plate structures quantitatively was developed by Sun et al. [10]. They introduced the damage with a circular/umbrella shape, so it did not precisely reflect the irregular surface damage. Hua et al. [11] proposed a new time–frequency damage index linking features extracted from Lamb wave signals for corrosion inspection applications. The significant second/third harmonics and the resonant waves were employed by Ding et al. [12] to investigate the surface corrosion damage in metal plates. Nicard et al. [13] used coda wave interferometry to monitor the generalized corrosion of steel strands. The problem of corrosion detection by using guided waves has also been widely described by Cegla et al. [14–18]. In [14], they estimated the accuracy of ultrasonically estimated corrosion rates (mean wall thickness loss) using standard signal processing methods based on the time of flight measurement (peak to peak, first arrival and the cross-correlation) and a novel thickness extraction algorithm (adaptive cross-correlation) has been presented. The potential of dispersive circumferential guided waves as a technique for screening or monitoring for pipe wall thinning due to corrosion was investigated in [15]. Next, the probability of detecting corrosion pits in pipes using circumferential guided waves was analyzed [16]. The fundamental S0, A0 and SH1 modes were used to monitor, inspect, or screen for finite areas of wall thickness change. An optimized ultrasonic corrosion monitoring technique for performing measurements in laboratory conditions has been described in [17]. The results show that wall loss rates of 0.1 mm/year to 0.2 mm/year could be detected within 1 h to 2 h, indicating that the developed technique is highly accurate and responsive. The reflection and scattering characteristics of shear bulk waves from corrosion pits have been investigated numerically in [18]. Many factors can influence the measurements, especially made in environmental conditions. Non-perfect transducer attachment due to. i.e., rough surfaces, initial thickness variations, presence of coating with different parameters, variations of material parameters, and possible mode conversions are not the only factors that can change the signal intensity, frequency content, and arrival time [19–22]. All these factors together mean that complete defect characterization of corrosion damage can be very challenging, and it is not always possible to determine the remaining plate thickness with any reliability.

This research paper introduces a novel method for assessing general corrosion levels. The main concept is based on estimating the symmetry level exhibited by the propagating wavefront. Despite that, the circular array of transducers for rapid localization and parametric identification of corrosion-type damage in metallic plates was investigated by Rathod and Mahapatra [23], and they also based their algorithm on the symmetry breaking in the signal pattern, their approach differs significantly from the method presented in this paper. The underlying concept assumes that thickness variations induced by general corrosion influence the wavefront circular shape. The common assumption that general corrosion causes uniform thickness reduction has been rejected. When the specimen's geometry becomes irregular, the wave propagation velocity becomes anisotropic, and the wavefront loses its circular shape.

Previous paper by the authors started considering random field modeling to assess the asymmetry of the ultrasonic wavefront in

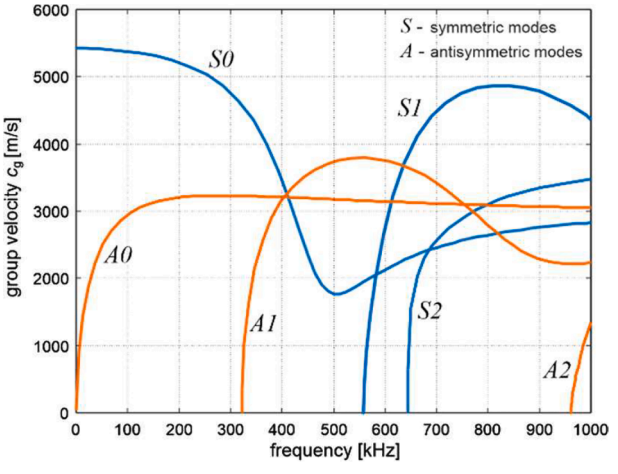

Fig. 1. Dispersion curves determined for steel plate ($E = 210$ GPa, $\nu = 0.3$ and $\rho = 7850$ kg/m^3) and constant thickness of $d = 5$ mm.

steel structures [24]. The present work investigates further this aspect by comprehensive experimental corrosion testing supported by ultrasonic gauge measurements. In addition, parametric numerical studies have been performed to assess the various degrees of degradation (DoD), the influence of the surface roughness on wavefield symmetry, and the frequency dependency via three different carrier frequencies. Experimental tests were complemented by numerical analyses conducted on plates with irregular surfaces modeled using random fields. An essential advantage of the proposed method over existing methods is the lack of necessity of exact mode identification and its lower sensitivity to systematic errors in time of flight (ToF) determination.

The paper is organized as follows: Section 2 introduces the theoretical background of wave propagation plates with variable thickness. The geometry of tested specimens and the methodology used is described in Section 3. The comparison of theoretical predictions with experimental and numerical results is provided in Sections 4 and 5. Finally, Section 6 contains the main discussion, conclusions, perspectives for future work as well as the limitations of the proposed method.

2. Theoretical background of wave propagation in plates with variable thickness

The influence of variable thickness has been widely investigated ([25–31]). Because of the dispersive character of guided waves, their propagation velocity depends on plate thickness. The dispersive equations were formulated by Lamb [32] and are derived for the uniform plate thickness, and their solutions are usually presented as dispersion curves. The exemplary solution is illustrated in Fig. 1, and the curves were traced for the steel plate with a thickness of 5 mm, considered in the further part of the paper.

Based on the dispersion curves, we can determine the group velocity c_g for the specific constant thickness d and estimate the time of flight (ToF) needed to travel along the distance L using a simple expression (Fig. 2a):

$$ToF = \frac{L}{c_g} \tag{1}$$

Unfortunately, the dispersion equations are formulated explicitly only for a few cases, like plates with constant thickness. In the case of plates with variable thickness, the above expression is not valid. The velocity along the propagation path in the complex plate with variable thickness also varies, which was demonstrated in [25,33,34]. The derivation presented in [33] by De Marchi et al. was made for tapered anisotropic plate with j segments with variable thicknesses d_j. They defined a group delay as a measure of the transit time versus frequency for a wave propagating along a waveguide. They considered the specimen with varying thickness and anti-symmetric wave propagation along the x direction (Fig. 2b), divided into N different uniform section divisions with a length Δl. The group delay of the m-th wave mode experiences in the i-th section of uniform cross-section and length Δl propagating between x_P and x_C can be calculated as:

$$gd^m_{x_P x_C}(f, L) = \sum_{i=1}^{N} \frac{\Delta l_i}{c^m_{gi}(f)} \tag{2}$$

where c^m_{gi} denotes group velocity of m-th wave mode determined for thickness d_i. The derivations and the results presented in the literature demonstrate that the wave velocity measured along distance L depends on the thickness variability which influences the group velocity c^m_{gi} [35] – this is basic assumption in this study.

This study focuses on the impact of general corrosion on guided wave propagation. Corrosion leads to complex plate geometries characterized by average thickness and standard deviation of thickness distribution. These parameters are crucial for estimating thickness reduction and are commonly used to assess degradation. While these parameters describe the overall surface, each propagation path between the actuator and sensor may have distinct statistical characteristics. With increasing irregularity due to corrosion,

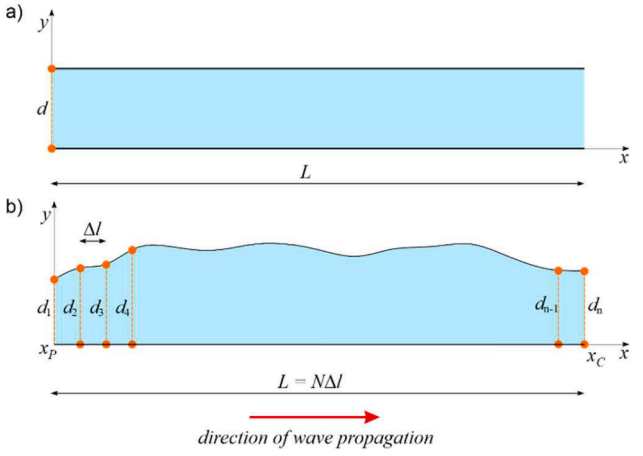

Fig. 2. The plates varying in thickness distribution: a) plate with constant thickness and b) plate with variable thickness.

variations in propagation paths become more significant, which is the primary assumption of the proposed method. Wave propagation velocity varies with thickness distribution, influencing different paths differently. The study investigates how thickness variability affects wavefront propagation, aiming to validate assumptions without solving an inverse problem.

3. Materials and methods

3.1. Experimental models of corroded plates

The experimental tests were conducted on a square steel plate with dimensions of 500 mm x 500 mm x 5 mm, and it was cut from the actual metal sheet prepared for ship structure repair and delivered from Remontowa Shipyard. The typical thickness of the ship hull is about 10 mm, but in extreme cases, it can range from 3 mm to even 650 mm [34]. A plate with a smaller thickness was selected to facilitate the experimental tests and achieve the expected corrosion level in a shorter time.

Controlled corrosion was induced via electrolysis reactions, employing an external power supply to drive ion movement. The plate was immersed in A 5 % sodium chloride solution, with direct current (DC) applied to accelerate corrosion, positioning the steel plate as the anode and another metal bar as the cathode. The accelerated corrosion test lasted 240 h, followed by drying. The corroded plate was subjected to nondestructive wave propagation tests and again subjected to electrolysis for another 240 h. The procedure was repeated until the required DoD (0 %, 10 %, and 20 %) was obtained (Fig. 3). Fig. 4 depicts the corrosion progression, showing significant increases in pit size and number as well as notable surface degradation.

Moreover, the photos of the plate corners at the beginning and end of the corrosion degradation process have been added. They clearly illustrate that the corners and edges are more prone to corrosion degradation, which is a common effect. This is also why the experimental test was conducted for three corrosion degradation levels. In the case of further electrochemical processes, the mass loss would be mainly associated with the degradation of the edges. At the same time, the middle part of the plate would be in much better condition and characterized by greater thickness.

Two different approaches were applied to assess the thickness reduction during anodic dissolution. First, weighting the dried, corroded plate has estimated the total mass reduction. It allowed for the estimation of the total DoD by using the expression:

$$DoD = \frac{m - m_{corr}}{m} \cdot 100\% \tag{3}$$

Next, ultrasonic gauge measurements were conducted. We used the calibrated device manufactured by Metrison SONO M660 to determine the thickness on a 50 mm mesh grid. The footprint probe was circular with an 8 mm diameter. In total, 121 measurements were made at each stage of the corrosion tests. This type of measurement was applied here because it is a common approach recommended, among others, by Classification Societies [36], defining the procedures of ship diagnostics. Ultrasonic gauge measurements will prepare the thickness variability maps, visualizing the progress and the nonuniform character of general corrosion.

A primary limitation of anodic dissolution lies in the inability to enforce a specific standard deviation of thickness distribution. Consequently, comparability of experimental signals is feasible solely for variable DoD, as the standard deviation acquired during ultrasonic measurement using an ultrasonic gauge is included solely for informational purposes. Fig. 5 illustrates thickness maps obtained through the standard ultrasonic gauge approach. A noticeable reduction in thickness is observed, particularly at the plate edges, which is a common occurrence. Given that the sensors are positioned in the middle section of the plate, the wavefront is exclusively influenced by thickness irregularities in this region. As a result, the thickness reduction at the plate edges does not impact the measured signals.

The analysis reveals that the undamaged plate exhibits surface irregularities. Table 1 consolidates the average thickness and standard deviation of thickness distribution for comparative purposes. These parameters are derived from measurements conducted at 121 points and offer a broad description of the surface characteristics. As the DoD increases, the standard deviation increases, which indicates that the corrosion degradation causes the surface to become more irregular. The standard deviation noted for the whole

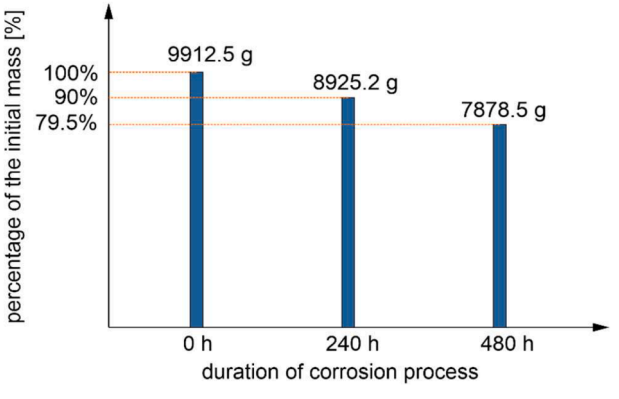

Fig. 3. Process of controlled corrosion: the mass reduction of the corroded plate.

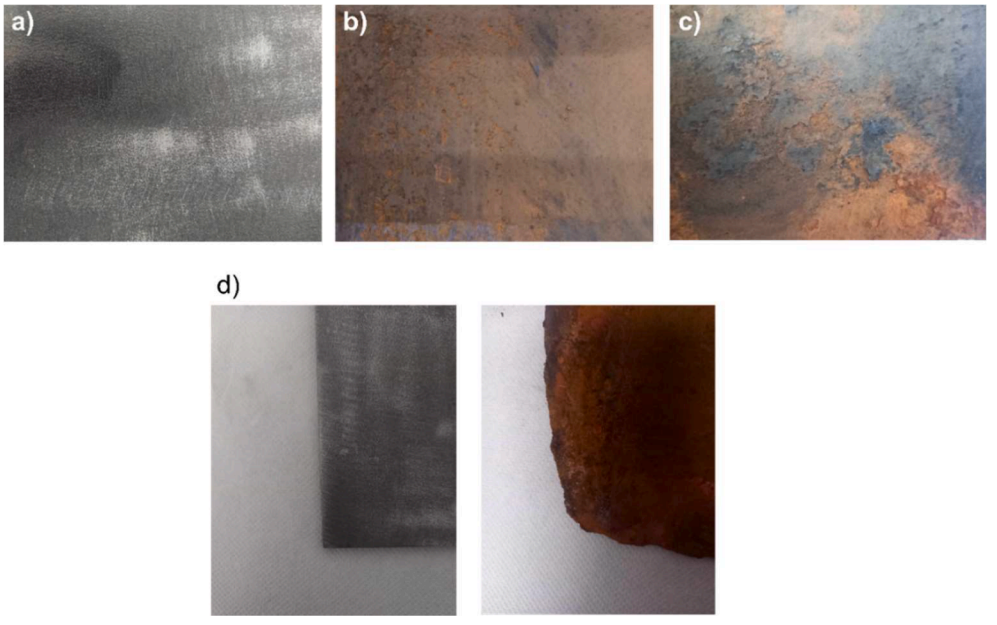

Fig. 4. Process of controlled corrosion: the photographs of plate surface with DoD of a) 0%, b) 9.96%, c) 20.52% and d) comparison of the plate corners at the beginning and the end of the corrosion process.

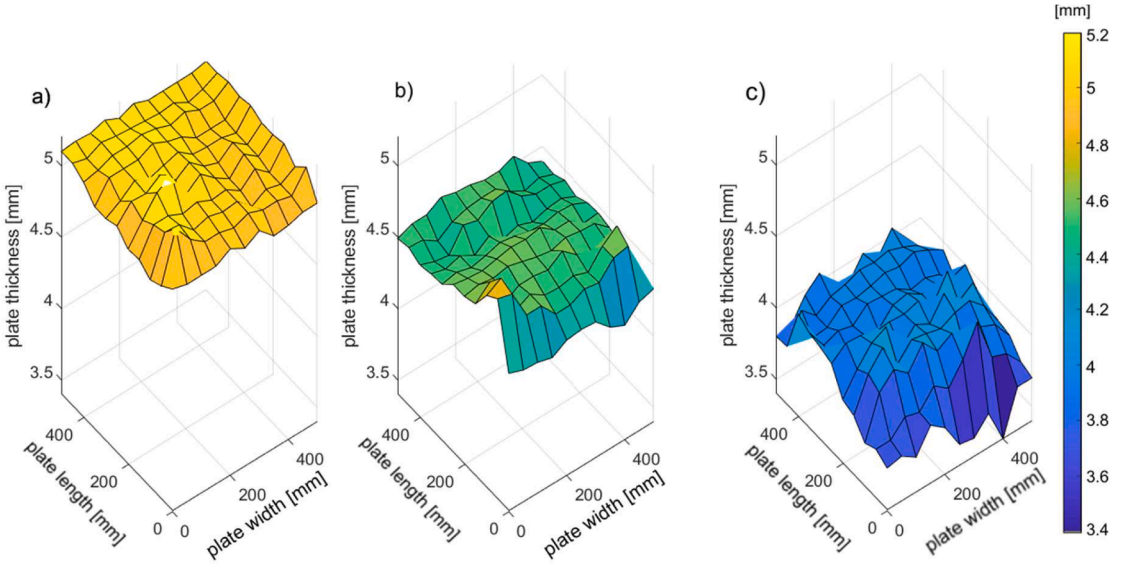

Fig. 5. Thickness map obtained during ultrasonic measurement.

Table 1
Surface parameters of experimental plates.

specimen	DoD [%]	average thickness [mm]	the standard deviation of thickness distribution [-]
#A	0	5.046	0.071
#B	10	4.501	0.100
#C	20	3.945	0.143

surface of corroded plates was 0.1007 and 0.143. If we consider only the middle part of the plate (area with dimensions of 30 cm x 30 cm, where in the following stages of the investigations, the sensors are mounted), the average thicknesses were similar (5.065 mm, 4.521 mm and 4.029 mm, respectively). Still, the surface was smoother, and the standard deviations of the thickness distribution

obtained for corroded plates were 0.053 and 0.0741. These values were next used as indicators for the values adopted for numerical simulations and random field generation.

The standard deviation obtained for uncorroded plate #A (0.071) is similar to that of the corroded plate #B (0.1). Usually, the corners and the edges are more prone to corrosion degradation, while the middle part remained smoother. Moreover, the deviation values in Table 1 were determined for the relatively sparse measurement grid, so they are only roughly estimated.

3.2. Experimental equipment

Fig. 6 illustrates the system used to conduct the experimental tests presented in this work. The guided waves were captured and excited by piezoceramic transducers with dimensions of 3 mm × 3 mm × 2 mm (NAC2024, Noliac). The transducers were adhered by wax, and they operated in pitch-catch mode. The excitation function was in the form of a five-cycle sine modulated by the Hann window:

$$p(t) = \begin{cases} 0.5p_0 \sin(2\pi ft)\left(1 - \cos\left(\frac{2\pi ft}{n_w}\right)\right) & t \in [0, T_w] \\ 0 & t \geqslant T_w \end{cases} \tag{4}$$

where f denotes the excitation frequency, p_0 is the excitation amplitude, the Hann window length, n_w and the number of time steps. The carrier frequencies were sent to the transducer via an arbitrary function generator (TiePie). The input excitation voltage after was 10 V, and the sampling frequency was defined as 10 MHz. At the same time, the transducers were connected to the high-voltage amplifier (Pendulum) to improve the signal-to-noise ratio (SNR). The output voltage after amplification of 10 times was equal to 100 V.

To facilitate the wavefront symmetry measurement, the circular array of 16 piezoelectric transducers was mounted on the plate surface (Fig. 6c and Fig. 7). They were attached to a circle with a radius of 15 cm. The actuator was located in the middle point of the plate, so each transducer was attached 15 cm away from the wave source. The reason for choosing the relatively high number of 16 transducers was the need to reconstruct the wavefront shape accurately. The distance of 15 cm between the sensors and the actuator was dictated by the size of the tested plate, which is 50 cm x 50 cm. The transducers were attached to the middle part of the plate to avoid the influence of edge reflections. Notably, in the case of the actual ship structures, they are often strengthened by stiffeners,

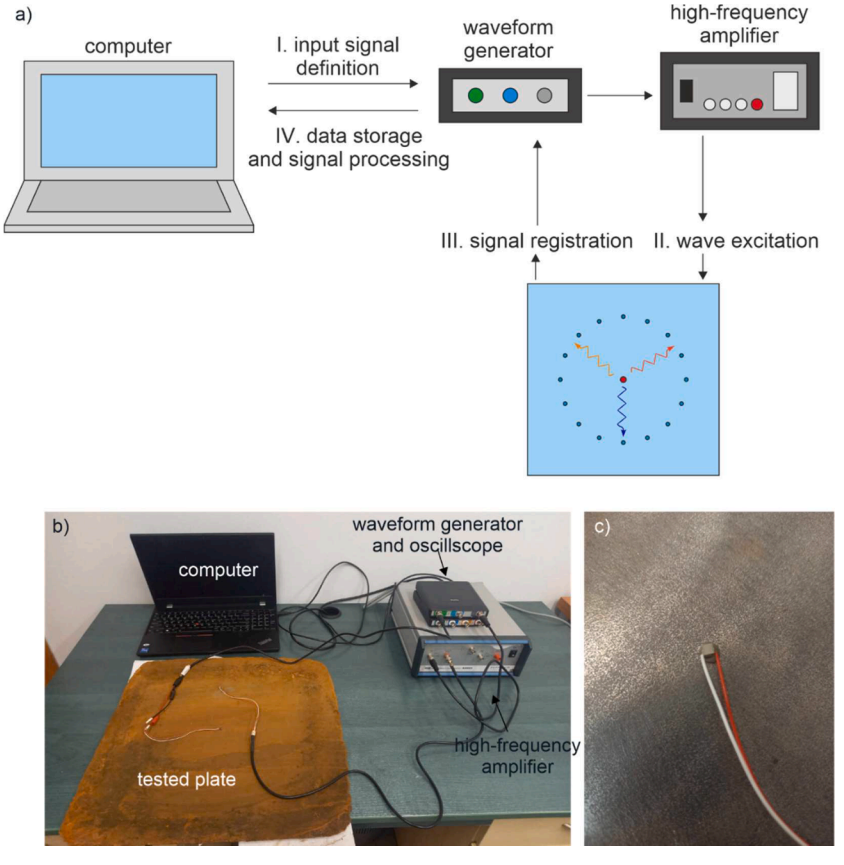

Fig. 6. Experimental investigation: a) the scheme of an experimental setup, b) the photograph of the setup, and c) the detail view of the transducer attachment.

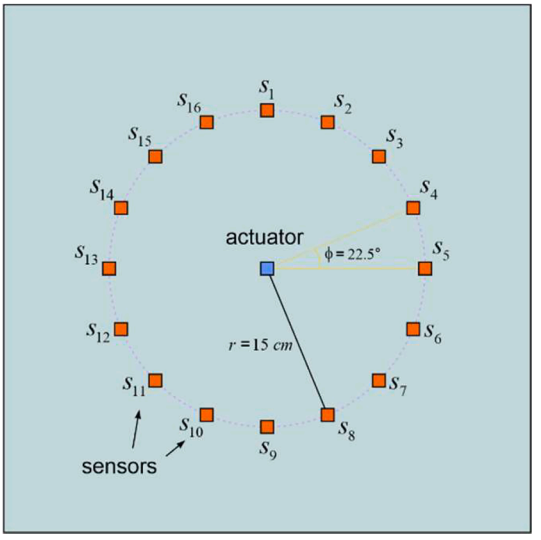

Fig. 7. Circular array of piezoelectric transducers.

which can also affect the registered signals. Therefore, the distance between transducers cannot be arbitrary but should be adapted to the structural geometry and the wave attenuation. Moreover, the size of the investigated plate and, as a consequence, the distance between the sensors were also determined by the complexity and time duration of the numerical analysis described in the next part of the paper.

The procedure of signal measurement involved recording and averaging 300 consecutive signals. Next, the average signal was filtered by a five-order Butterworth band-pass filter with cut-off frequencies at 20 and 2*f* kHz, where *f* is the excitation frequency [37]. The signals were cross-correlated to calculate the ToFs of the first propagating mode, which were further used to reconstruct the wavefront shape.

The sensitivity analysis has preceded both numerical and experimental tests to choose the appropriate wave mode. Because the compressive type transducers attached to the plate surface have been used, the A0 mode has been excited mainly. However, the frequencies for which A0 was pronounced and the high SNR were selected to facilitate further signal processing. To do this, the variable frequency signals were collected, and their amplitude and readability were compared. In this study, the frequencies below 150 kHz were characterized by the highest SNR. To investigate the influence of the excitation frequency on the obtained results, 50, 100, and 150 kHz were used as carriers.

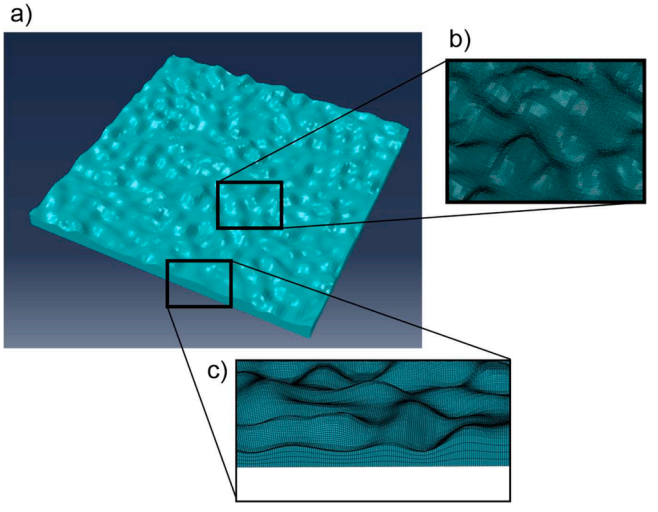

Fig. 8. Numerical simulations performed in Abaqus software: a) model of the corroded plate, b) zoom of the plate surface, and c) view of the variable thickness of corroded plate.

3.3. FE modeling

Numerical models were performed using the commercial software Abaqus/Explicit (Fig. 8). The plates were modeled as 3D objects built of 8-node brick elements with reduced integration (C3D8R). The time step equal to 10^{-8} s and the element's size not exceeding 0.5x0.5x0.5 mm^3 were adjusted to the excitation frequency range and the wavelength to satisfy the Courant–Friedrichs–Lewy conditions. The time duration of the analysis was equal to 0.5 ms. The excitation was applied as a time-dependent force in the plate's middle point (Eq. (4)). Because of the high stiffness of the actuator (115.00 N/μm), the actuation was replaced by the time-dependent concentrated force of 1 N applied in the middle point of the plate [38]. This simplification causes only the local, close to the excitation point inaccuracies of simulation, which is not considered here. The time course of the excitation corresponded to experimental data. The out-of-plane displacement components associated with A0 mode were registered in selected model nodes corresponding to the exact positions of the transducers during experimental tests. The material parameters adopted in the model were typical for steel: elastic modulus $E = 210$ GPa, Poisson's ratio $\nu = 0.3$, and density $\rho = 7850$ kg/m^3. Despite the high calculation cost, the numerical simulations were performed for the 3D models as the plain strain conditions would not provide the possibility to model the surface roughness and observe the differences in wave propagation in various directions.

We harnessed stochastic processes known as random fields to simulate corroded surfaces, as the pits occur randomly. Random fields are commonly employed due to their robustness in modeling spatial distributions [39,40], offering a diverse range of options such as Markov random fields (MRF), Gibbs random fields, conditional random fields (CRF), and Gaussian random fields (GRF). Gaussian random fields, particularly notable, produce irregular yet continuous surfaces, employing Gaussian probability density functions. Our study used MATLAB and the Karhunen-Loeve (KL) expansion algorithm [41] to simulate rough surfaces, specifying dimensions and truncation levels for polynomial KL expansion. Principal considerations encompass the specification of the random field's dimensions. Our endeavor commenced with a mesh measuring 100x100 units, a choice aimed at ensuring computationally feasible processing durations. Another pivotal parameter is truncation, for which we established various levels of polynomial KL expansion. Furthermore, the interrelation between mesh points is dictated by a predetermined value. By fine-tuning these parameters, we successfully simulated corroded surfaces by applying truncated Gaussian distribution within the overarching framework of random fields.

In the first step, the numerical plate models were defined as undamaged, smooth plates with constant thickness. Next, the input file was modified, and the mesh nodes were moved to adjust their coordinates to the generated random field performed in the MATLAB environment.

3.4. Considered numerical models

The numerical models considered within this study are summarized in Table 1. The degree of degradation varied from 0 to 60 %. For each DoD, the various values of standard deviation of thickness distribution were additionally considered for random field generation. The simulations were performed for σ equal to 0.05, 0.1, 0.15 and 0.2. The exception was DoD of 10 %, for which the standard deviation was equal to 0.05 or 0.1. For the higher values, the maximum resulting thickness of the corroded plate would be greater than the maximum thickness of the undamaged plate, which has no physical sense. To investigate the influence of the excitation frequency, the signals were collected for frequencies 50, 100, and 150 kHz. In total, 69 models were considered, and 1104 signals were processed

Table 2
Numerical models considered within the study. Each model has been simulated for three frequencies (50 kHz, 100 kHz, 150 kHz).

specimen group	degree of degradation DoD [%]	standard deviation σ (compared to the initial thickness)
A#	0	0
B#	10	0.05
		0.1
C#	20	0.05
		0.1
		0.15
		0.2
D#	30	0.05
		0.1
		0.15
		0.2
E#	40	0.05
		0.1
		0.15
		0.2
F#	50	0.05
		0.1
		0.15
		0.2
G#	60	0.05
		0.1
		0.15
		0.2

(see Table 2).

The range of the DoD is wide – DoD of 60 % is considered excessive and dangerous for structural safety. However, in extreme cases, the DoD may exceed 50 % [42,43]. Moreover, to better understand and observe the trend of the symmetry degrees for increasing DoD, we decided to investigate a numerically more significant number of cases, even if the DoD of 60 % is less likely for regularly inspected ships and offshore structures.

3.5. Wavefield symmetry assessment

To assess the symmetry of the propagating wavefront, the first necessary step is to reconstruct its shape based on the signals registered by the sensor network. To do this, the following procedure has been developed:

1) Attach the transducers at equal distances r from the actuator and record the signals;
2) Identify the selected wave mode and determine its ToF (in this article, we consider the incident A0 mode);
3) Calculate the lengths along which the wavefront extends (determine the velocities in particular directions and next calculate the distances which were traveled in the minimal ToF):

$$v_k = \frac{r}{ToF_k} \tag{5}$$

$$r_k = v_k \cdot \min\{ToF_i\} \tag{6}$$

where k is the number of transducers, and i is the total number of transducers. The reconstructed wavefront was spread over i arms of lengths r_k. The obtained shape is denoted as M in the further considerations. The scheme of wavefront reconstruction is presented in Fig. 9.

This presented evaluation of corrosion-related deterioration relies on examining bilateral and rotational central symmetry degrees [24,44]. Consider a shape denoted as M in the Euclidean space R^2 (Fig. 10). Concurrently, let M' symbolize the shape resulting from applying ith rotation operations to the original shape M. The rotation angle is denoted as α. Similarly, M'' signifies the shape achieved by reflecting shape M' across the specified x-axis. When defining the bilateral central symmetry degree, labeled as $BCSD(i)$ concerning the x-axis, it is established as the proportion of the area denoted as A, corresponding to the overlapping region between shape M' and its mirrored counterpart M'', relative to the total area occupied by shape M:

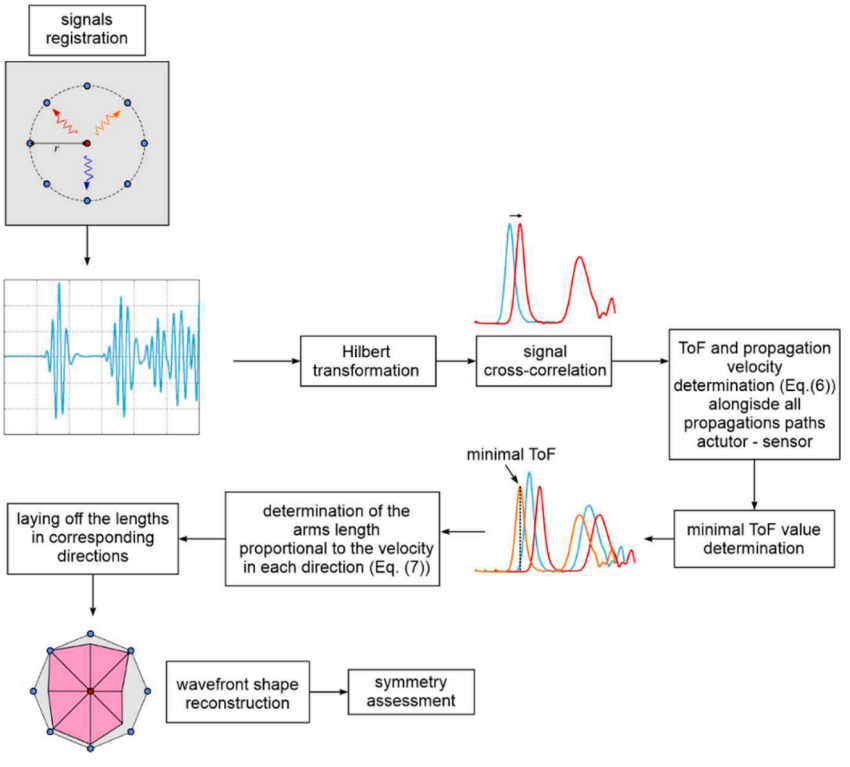

Fig. 9. The procedure of wavefront reconstruction based on ToF.

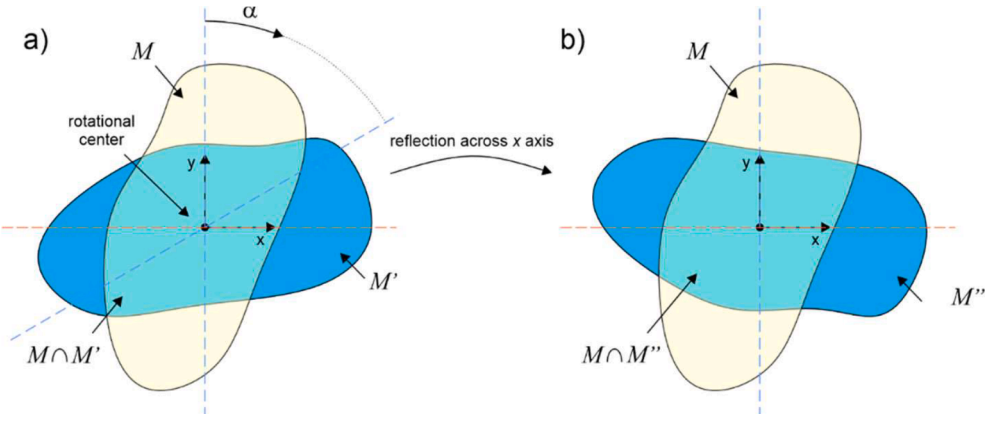

Fig. 10. The procedure of calculation of a) rotational symmetry degree and b) bilateral symmetry degree.

$$BCSD(i) = \frac{A(M_i' \cap M_i'')}{A(M)} \tag{7}$$

We can also establish the bilateral symmetricity of a given shape M denoted as δ_B, which corresponds to the highest achievable value of the bilateral central symmetry degree:

$$\delta_B = \max\{BCSD(i)\} \tag{8}$$

This value falls within the range of 0 to 1, with $\delta_B = 1$ indicating a state of perfect bilateral symmetry within the shape. By searching $\delta_B = 1$, we can ascertain the count of axes that exhibit perfect bilateral symmetry.

The ratio of the area of the intersection of the initial shape M and the rotated shape M' is defined as the rotational symmetry degree:

$$RCSD(i) = \frac{A(M \cap M_i')}{A(M)} \tag{9}$$

and the maximum value of the rotational central symmetry degree is the rotational symmetricity of a shape M and is denoted as δ_R. Because the value of RCSD is equal to 1 for an angle 0 and 2π they represent pseudo-data, which have to be discarded. The discarding procedure can be summarized in the following steps (Fig. 11): find the first local minimum of RCSD noted l_1 and then find the last local minimum denoted as l_2. Discard the data close to 0 ($i < l_1$) and data close to 2π ($i > l_2$) and determine the rotational symmetricity, taking into account the non-discarded data.

4. Numerical results

4.1. The influence of DoD on wavefield symmetry

In the first step, we consider the influence of the average mass loss on the wavefront shape. The visualization presented in Fig. 12 depicts the wave propagation field at selected time instants obtained for plates varying in DoD. The snapshots were performed for four

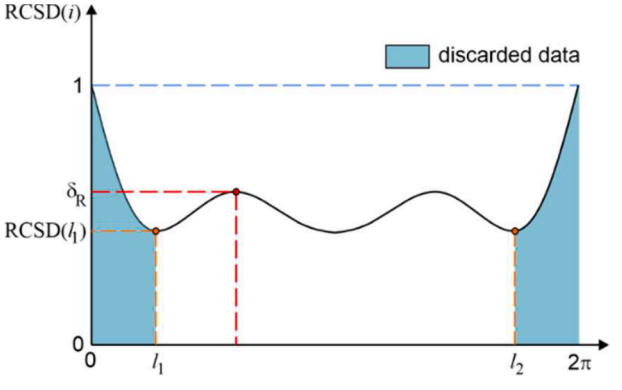

Fig. 11. Determining the rotational symmetricity from the RCSD plot [44].

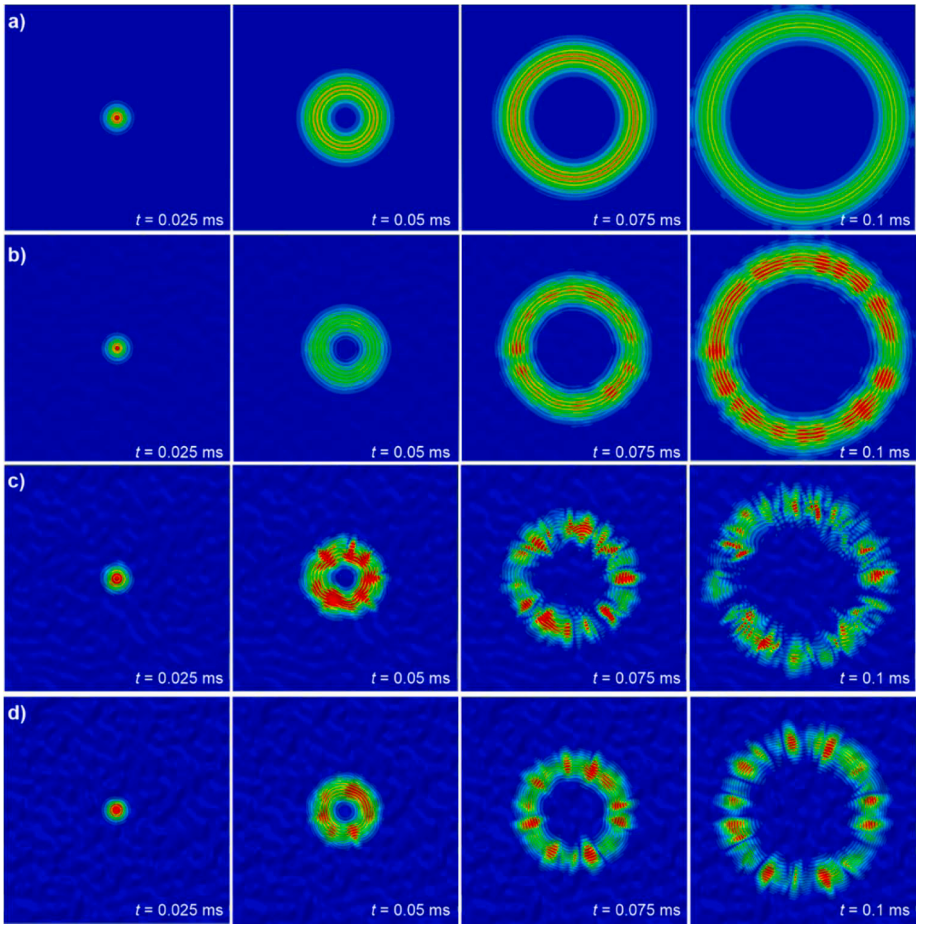

Fig. 12. Visualization of wave propagation in steel plates varying in DoD: a) undamaged plate with DoD of 0%, b) plate with DoD of 20%, c) plate with DoD of 40% and d) plate with DoD of 60% and a standard deviation of 0.1.

models (A#, C# E# and G#) with the same standard deviation of thickness distribution and an exemplary frequency of 100 kHz. Even based on the visualization, the impact of corrosion degradation on the propagating wavefront is visible. Two main aspects should be noted here. First of all, the wavefront loses its circular symmetry with increasing DoD. In a perfect, undamaged isotropic plate with constant thickness, the wavefront is circular as the wave propagates with the same velocity in each direction. In the case of damaged plates, the thickness is variable, and in consequence, the velocity differs along the propagation paths, and the shape of the wavefront differs. However, one can notice an additional effect related to the area of the field swept by the wavefront. Due to thickness reduction, the propagation velocity decreases; thus, the lengths of the propagation paths are shorter. One can see that the surface roughness also

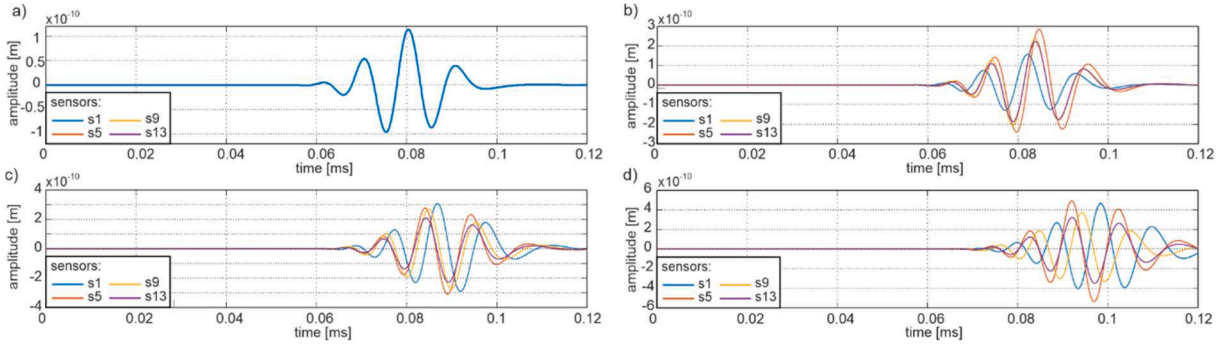

Fig. 13. Exemplary wave propagation signals obtained for variable DoD: a) DoD = 0 %, b) DoD = 20 %, c) DoD = 40 % and DoD = 60 % for a frequency of 100 kHz (the standard deviation of thickness distribution was the same in all cases and it was 0.1).

influences the symmetry of the amplitude, but this parameter is not considered in this study.

Fig. 13 demonstrates the calculated wave propagation signals for considered plates. The signals represent the displacements measured perpendicular to the plate surface. For readability, only the signals captured by four sensors 90 degrees apart (sensors 1, 5, 9, and 13) were plotted in the graph. The time range was adjusted to demonstrate only incident waves without edge reflection. As mentioned, in the case of a perfect plate, we can observe the ideal symmetry of the propagating wavefront. The signals collected in Fig. 13a obtained for plates with DoD of 0 % (undamaged) coincide perfectly with each other and are characterized by the same time course and the amplitude of particular wave packets. The signals registered for corroded plates (Fig. 13b-d) differ in the ToF of individual wave packets. One can see that even though the DoD and the standard deviation of thickness distribution were defined for the whole plate, the ToF, and the signal characters differ for various directions. This confirms the primary assumption made in this study: that corrosion degradation affects not only the average wave propagation velocity because of thickness reduction but also the symmetry of wave motion in the plate.

To demonstrate the influence of thickness reduction on the average wave velocity, the average ToF for all sensors was calculated in the first step. The results are given in Fig. 14. Additionally, the theoretical predictions made using dispersion curves were plotted for comparison. It is worth noting that the theoretical ToFs were determined for the average thickness reduction. The correspondence of the numerical ToFs averaged from 16 signals and the theoretical ToFs determined for plates with constant average thickness clearly indicates that the proposed method is also suitable for assessing the average DoD. The progress of corrosion degradation is associated with increasing ToF – the slope of the curve is higher for 50 kHz, which corresponds with the most significant slope of the dispersion curve for this frequency (Fig. 1) and, consequently, in the highest sensitivity to the thickness reduction. Although the proposed approach is based on symmetry degree assessment and the circular array of the transducers was chosen to facilitate the reconstruction of the wavefront shape, the determined ToFs can also be used to control the average thickness reduction.

Next, the signals collected were processed using the procedure described in Section 3.5, and the wavefront shapes were reconstructed (Fig. 15). Additionally, the procedure of wavefront comparison is illustrated in the figure. The origin of the coordinate system is associated with the actuator position, so the extreme positions of the transducers on x and y axes are 0.15 m and −0.15 m. The wavefront shape marked orange represents the wave propagating in the undamaged, smooth plate. The grey shape represents a wave spreading in the corroded plate. In each case, the grey shape is characterized by a smaller area than the orange one, associated with lower wave velocity in the corroded plate. However, one can see that the visual assessment of the corrosion degradation process based only on comparing the wavefronts obtained for plates varying in DoD would be challenging because the differences in particular wavefront shapes are insignificant.

To quantitatively analyze the effect of DoD on wavefront symmetry degrees, in the following figures, the RCSD (Fig. 16) and BCSD (Fig. 17) functions were plotted for all considered cases, and the values for central symmetry degrees were also determined. For readability and simplicity, all the functions are presented only at the beginning, while in the following sections, only maximal and minimal degrees of symmetry will be considered. Each column contains the results obtained for different frequencies from 50 to 150 kHz, while each row contains the results for variable DoD. Each graph presents four functions (or two for DoD of 10 %) for the various standard deviations of thickness distribution.

We can clearly see that the DoD significantly influences obtained symmetry degree functions. In both BCSD and RCSD, the functions have smaller values for increasing DoD, and additionally, in the case of BCSD, the functions lost their regularity (see Fig. 17a and d).

From a practical point of view, detecting corrosion early in its development is crucial. Therefore, in Fig. 18 and in Fig. 19, the RCSD and BCSD functions were plotted for DoD varying only in a limited range from 0 to 20 % and for the standard deviation of the thickness distribution of 0.1, which also facilitates the comparison. Regardless of the symmetry type, a similar effect is observed in both cases. For the perfect plate, the number of peaks reaching 1 is equal to the number of the transducers (16), and they appear every 22.5°, which corresponds to their spacing, similarly to the local minima. When DoD increases, the character of the functions does not vary

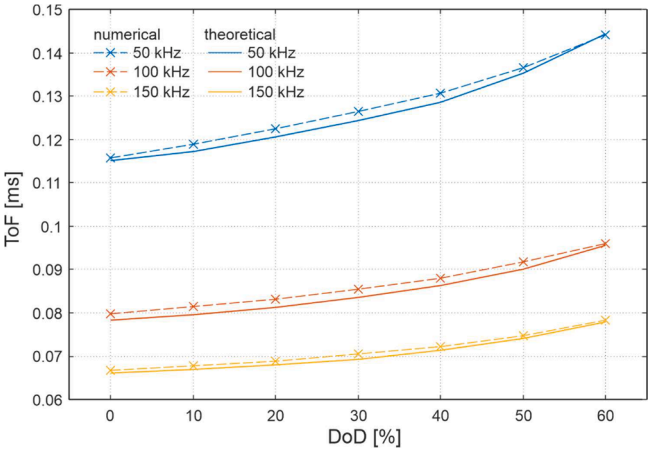

Fig. 14. Average ToF determined for signals registered by 16 sensors – the results are presented for the corroded plates with irregular surfaces characterized by a standard deviation of 0.1.

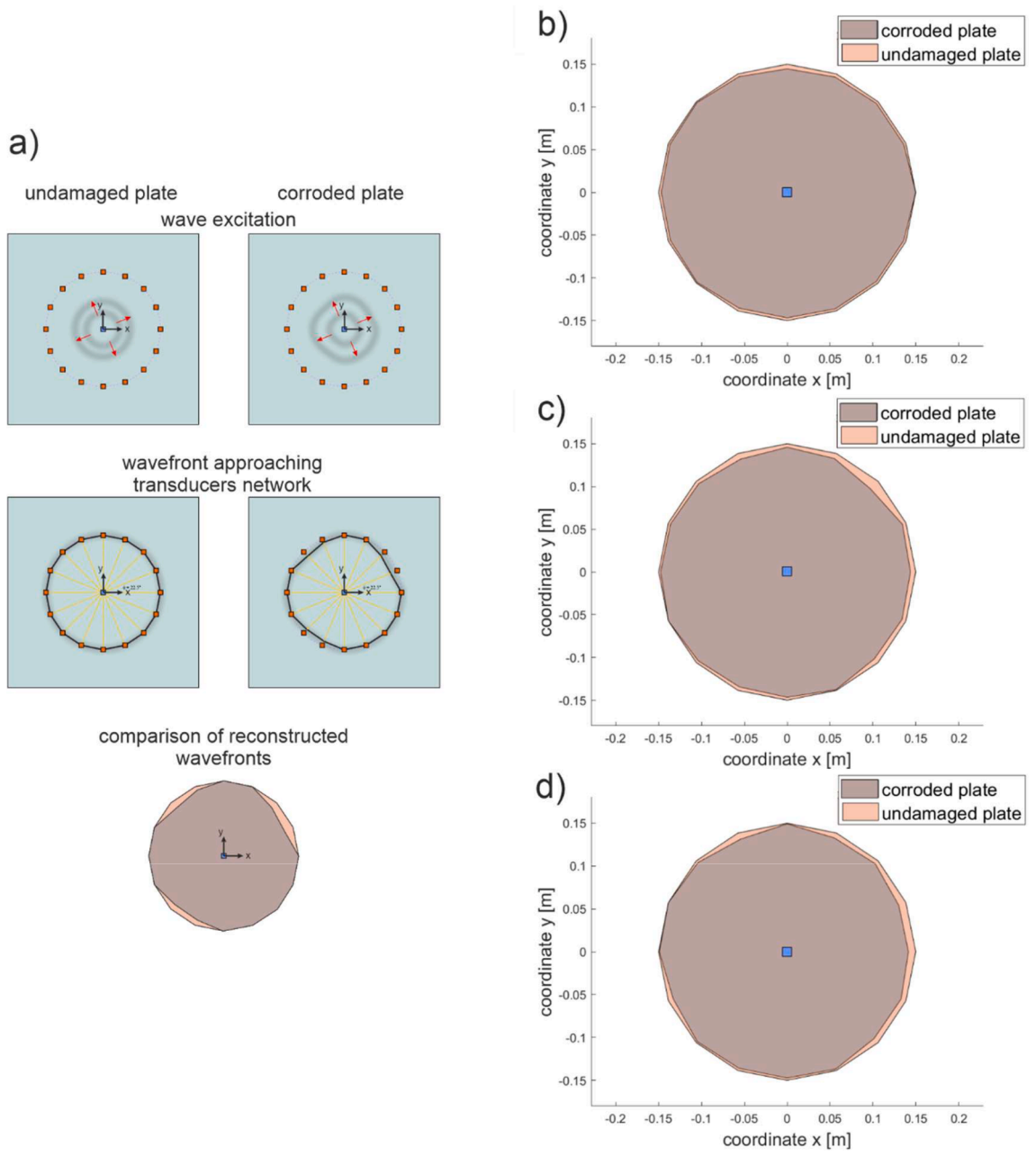

Fig. 15. Exemplary reconstructed wavefronts for variable DoD (in each case, the excitation frequency was equal to 100 kHz, and the standard deviation of thickness distribution was 0.1 of initial thickness): a) procedure of wavefront comparison and wavefronts for a) DoD of 20 %, b) DoD of 40 % and c) DoD of 60 % compared with the wavefront obtained for undamaged plate.

significantly. The number of maxima and minima and the frequency of their occurrence remain the same, but the value decreases.

Moreover, the decrease of RCSD and BCSD functions is more visible for DoD, increasing from 0 % to 10 % than for the increase from 10 % to 20 %. This may be associated with the symmetry being more sensitive to the surface roughness. In the case of plate, A# the standard deviation of the thickness distribution was equal to 0, while in the case of plate #B and #C the surface roughness was comparable, and the standard deviation was non-zero ($\sigma = 0.1$). The results suggest that monitoring bilateral or rotational symmetry can be especially useful in an early stage of corrosion degradation when the surface significantly changes its morphology or in late corrosion assessment when the propagating wavefront totally loses its symmetry.

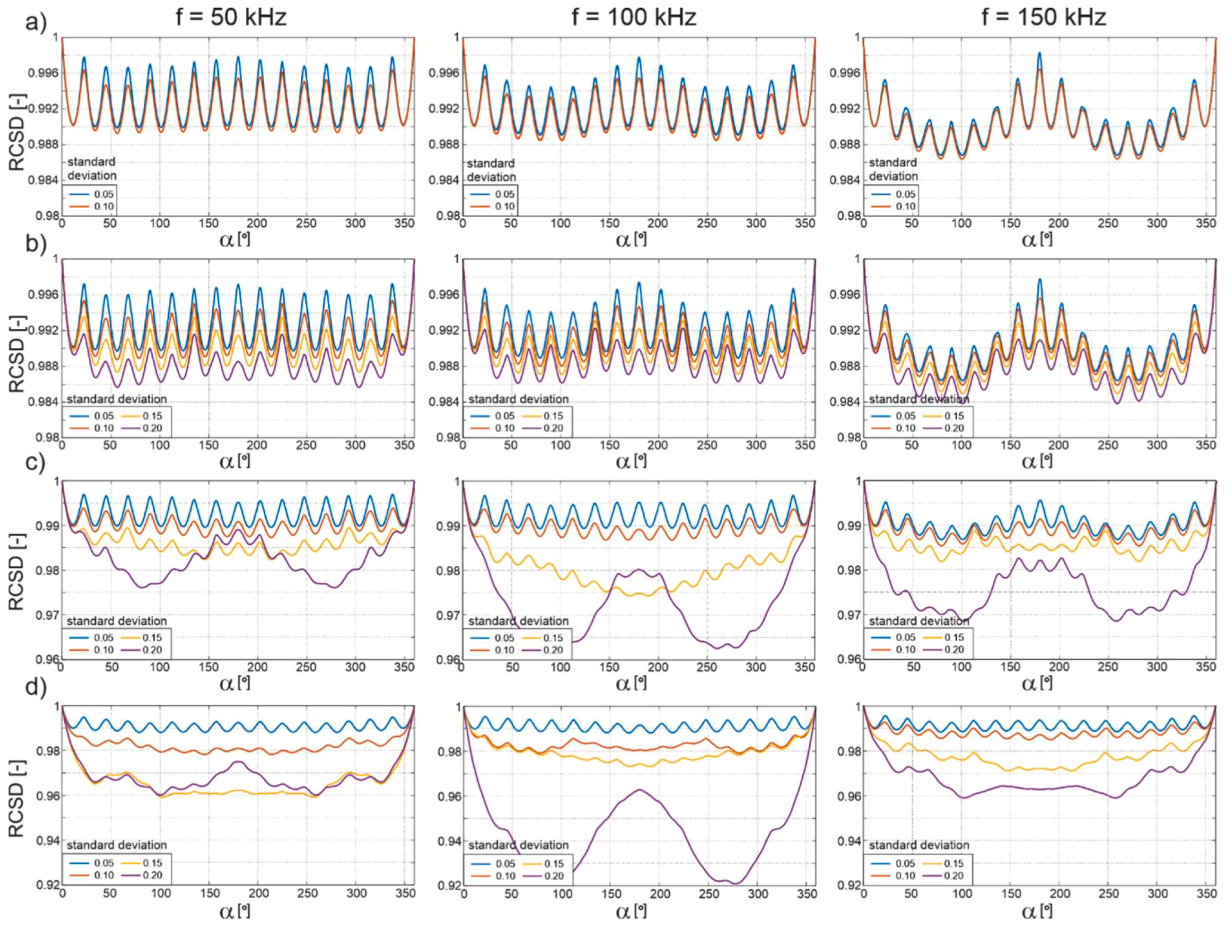

Fig. 16. RCSD functions determined for plates varying in DoD: a) 10%, b) 20%, c) 40% and d) 60% obtained for different excitation frequencies and standard deviations of thickness distribution.

4.2. The influence of standard deviation of thickness distribution on wavefield symmetry

The minimal and maximal values of BCSD and RCSD functions have been determined in each case and presented in figures (Fig. 20–23). Moreover, in each case, the minimal and maximal values of the symmetry degrees were determined for perfect and undamaged plates. The figures indicated their values by straight dashed lines (grey line A for minimal values and green dashed line B for maximal values). The maximal value for the undamaged plate is always equal to 1, which means that the rotated and/or reflected shape perfectly covers the initial shape of the wavefront. However, the minimal value is determined by the number of sensors incorporated in the network, increasing with the extent of the network. For the network built of 16 sensors, it is equal to 0.9903.

The results indicate that the standard deviation of thickness distribution, which is the roughness of the surface, has a noticeable influence on the wavefront symmetry. The increase of standard deviation results in more significant variability of wave propagation velocity and, consequently, lower values of symmetry degrees. The comparison of the symmetry functions obtained for DoD varying from 0 to 20 % revealed that roughness is the crucial parameter that affects wavefront symmetry (Fig. 18 and Fig. 19). However, as mentioned, this effect is pronounced for higher DoD: for DoD of 20 %, the decrease in symmetry degrees is observable, but their values are comparable for different surface roughness. The differences in symmetry degrees obtained for DoD of 60 % and for variable roughness are easily noticeable. The explanation for this is the increasing slope of the dispersion curve for smaller plate thicknesses. As the DoD increases and *fd* product decreases, we move toward the beginning of the dispersion curve representing A0 mode, characterized by the significant slope (Fig. 1). This means that for higher DoD, each deviation from the average thickness is associated with a more considerable velocity change, regardless the excitation frequency. Therefore, increasing of the standard deviation of the thickness distribution has a more significant influence on wavefront symmetry in thinner plates.

This observation that not only DoD but also the geometry and the surface shape influence wave propagation velocity is crucial because we can measure precisely the same velocity for two different plates varying in DoDs because of the effect of surface roughness. This observation proves that the so far applied approach based on estimating the average thickness based on average wave velocity measured along the propagation path may be affected with significant inaccuracies. A possible solution for separating the DoD and roughness effect is to simultaneously analyze average velocity (Fig. 14) together with symmetry degrees.

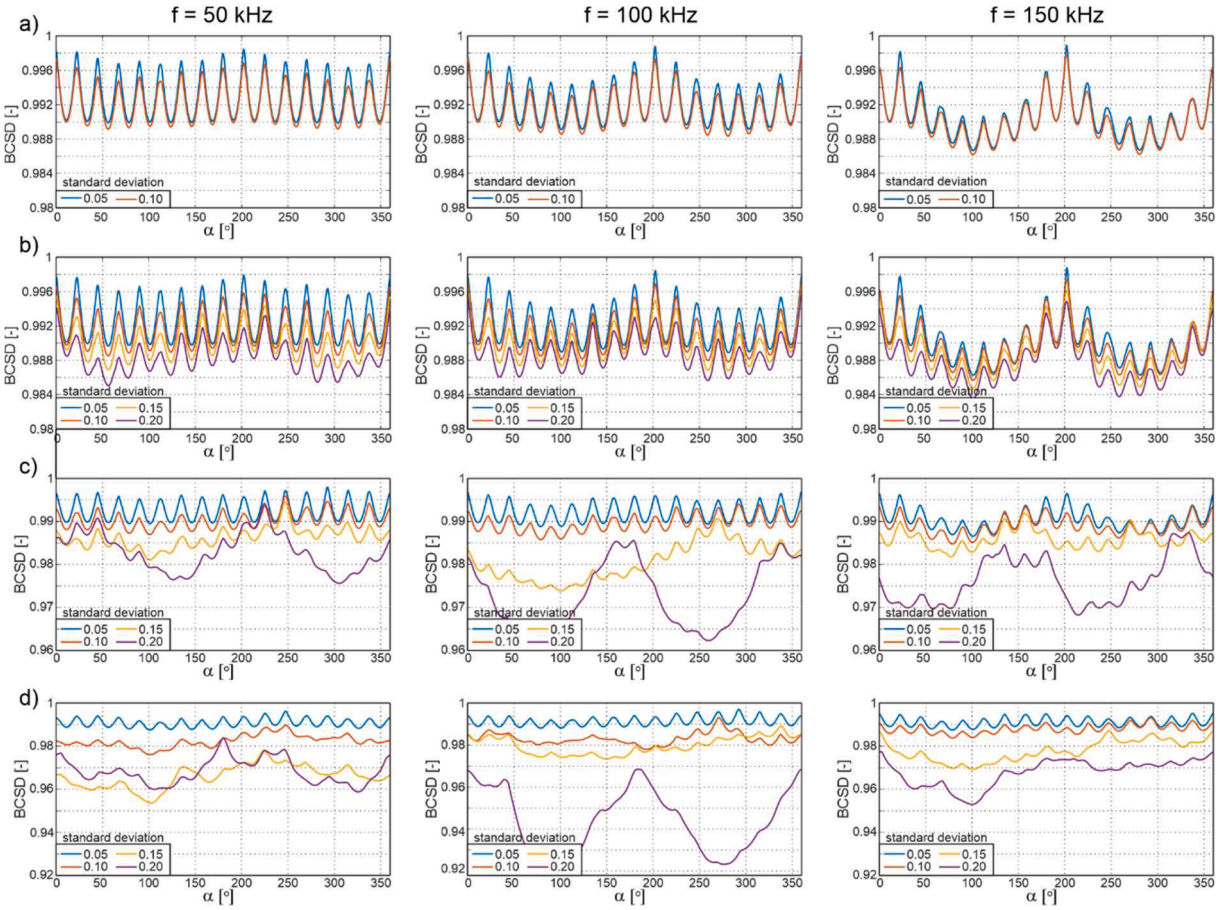

Fig. 17. BCSD functions determined for plates varying in DoD: a) 10%, b) 20%, c) 40% and d) 60% obtained for different excitation frequencies and standard deviations of thickness distribution.

4.3. The influence of the excitation frequency on central symmetry degrees

The excitation frequency impacts the shape of the BCSD and RCSD functions (Fig. 16 and Fig. 17), but it is less visible when the extreme values of symmetry degrees are compared (Figs. 20–23). In the case of all frequencies, the maximal and minimal values of symmetry degrees were comparable for the same DoD. On the other hand, one can see that the higher frequencies (100 and 150 kHz) gave unambiguous results in all cases, i.e., the increase of DoD or standard deviation always resulted in increasing values of RCSD and BCSD. In contrast, for the lowest frequency considered here, i.e., 50 kHz, the results were not unambiguous in each case, especially for the significant DoD. Notably, the course of function has been disturbed for the most corroded plates with DoD of 50 % and 60 %. Although we consequently observed the increase of BCSD and RCSD with increasing degradation, this trend is disturbed for plates F and G with standard deviations of 0.15 and 0.2. Despite the lower standard deviation value, we noted a higher value of symmetry degrees (Fig. 20a – Fig. 23a). This effect was observed only for a frequency of 50 kHz with the greatest wavelength. As mentioned above, the decrease of *fd* product is associated with an increasing slope of the dispersion curve and higher sensitivity to thickness variations. On the other hand, if the decrease of *fd* product is caused by applying lower frequency (not thickness reduction), we also need to consider the increasing wavelength, which is generally less sensitive to insignificant thickness changes and surface roughness. Therefore, it is possible to note the ambiguous results for the lower frequencies.

5. Experimental results

The piezo transducers were attached in a circular array in the next step, and the guided waves were excited. The exemplary signals measured by four sensors (s1, s5, s9 and s13) for DoD of 0 %, ~10 % and ~ 20 % are given in Fig. 24. The main difference between theoretical predictions and experimental measurements is the lack of perfect correspondence between the signals measured for the undamaged plate. In the case of the numerical model, the signals registered at the same distance from an actuator were the same (compare Fig. 13). Despite significant similarity, the difference between the amplitude and the ToF is observable in the case of experimental tests. The main reason for these differences is the difference in transducer attachment. In the experimental test, the wax

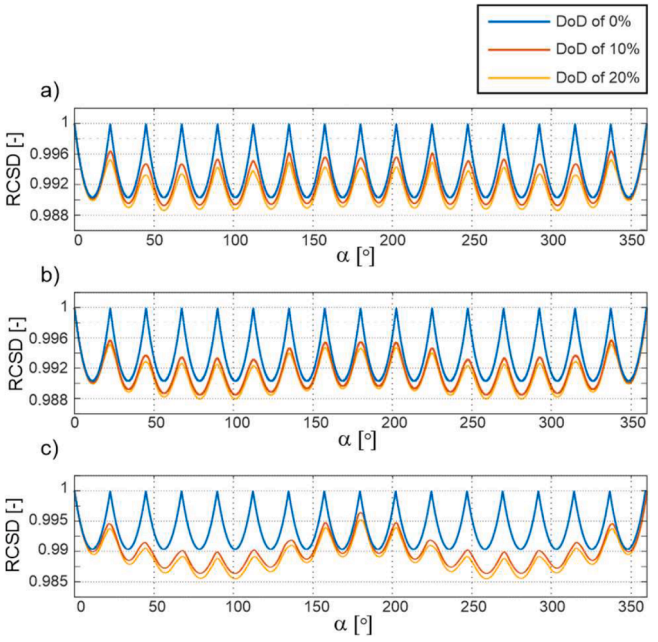

Fig. 18. RCSD functions determined for plates varying in DoD: a) RCSD determined for excitation frequency of 50 kHz, b) 100 kHz and c) 150 kHz.

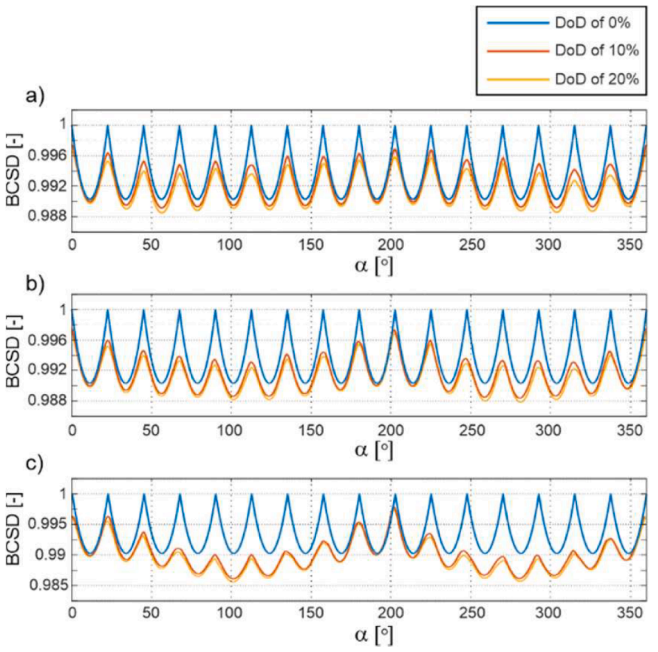

Fig. 19. BCSD functions determined for plates varying in DoD: a) RCSD determined for excitation frequency of 50 kHz, b) 100 kHz and c) 150 kHz.

was used to mount the transducers. Its main advantage was the possibility of removement before immersion in electrolyte and accelerated corrosion. However, the wax amount and its consistency affect the signals' amplitude. Therefore, we observe the amplitude variability because it depends on the mounting method, amount of wax, etc. The second reason for the difference in measured signals is the accuracy of the transducer's attachment. Despite meticulous care in the experimental tests to ensure precise sensor mounting, there is a potential for subtle deviations in the sensor attachment locations. Measuring the distance between the actuator and sensor employed conventional measuring equipment, precisely a tape measure, with an associated measurement accuracy of $\pm$ 1.2 of the smallest division on the scale equal to 0.5 mm. In the presented study, the experimental tests were repeated for each case, and the difference in the ToFs because of the accuracy of the transducer's attachment obtained for the corresponding sensors was

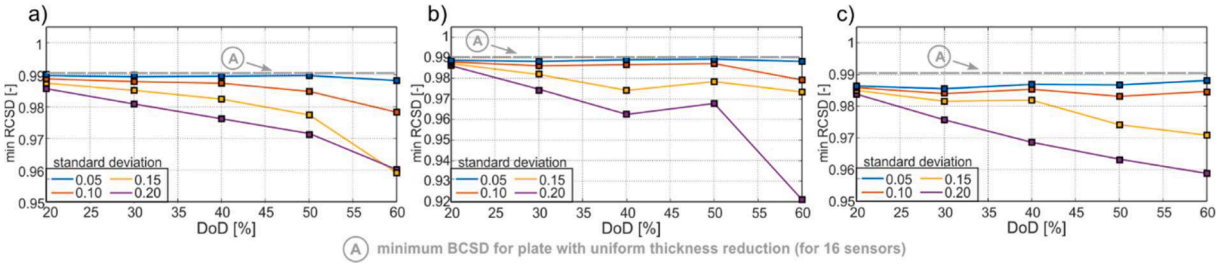

Fig. 20. Minimal values of RCSD functions determined for plates varying in DoD and for various excitation frequencies a) 50 kHz, b) 100 kHz and c) 150 kHz.

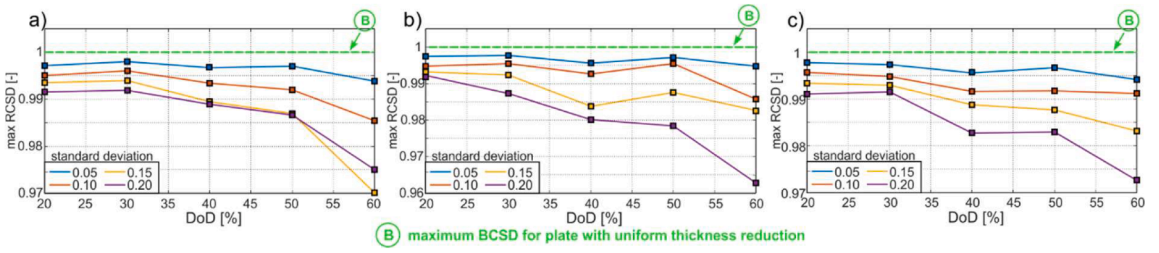

Fig. 21. Maximal values of RCSD functions determined for plates varying in DoD and for various excitation frequencies a) 50 kHz, b) 100 kHz and c) 150 kHz.

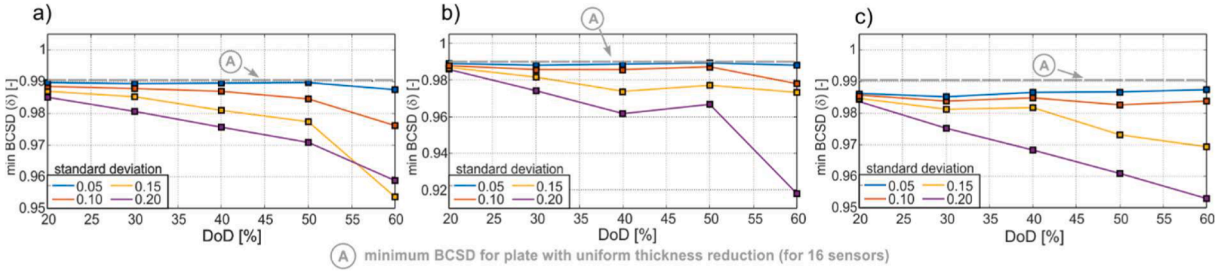

Fig. 22. Minimal values of BCSD functions determined for plates varying in DoD and for various excitation frequencies a) 50 kHz, b) 100 kHz and c) 150 kHz.

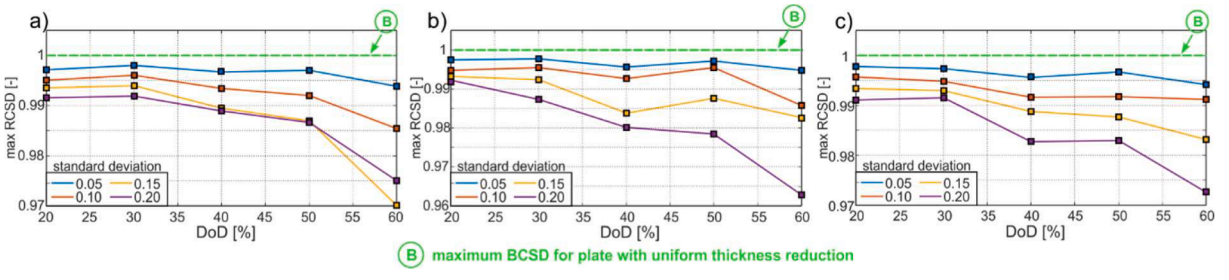

Fig. 23. Maximal values of BCSD functions determined for plates varying in DoD and for various excitation frequencies a) 50 kHz, b) 100 kHz and c) 150 kHz.

not greater than 0.85 % of the average ToF for 50 kHz, 0.86 % for 100 kHz and 1.5 % for 150 kHz. The difference in ToF has been calculated as the difference between maximum and minimum ToFs obtained for selected transducers during five experimental campaigns conducted on undamaged plate. The most significant error in the case of the highest frequency is caused by the shortest duration of the wave packets, higher signal resolution and the greater number of peaks registered in the signal. The influence of the measurement accuracy on the wavefront asymmetry should be addressed in detail in the future.

The geometric irregularities also impact the undamaged plate's measured signals. Even in the case of a structurally sound plate,

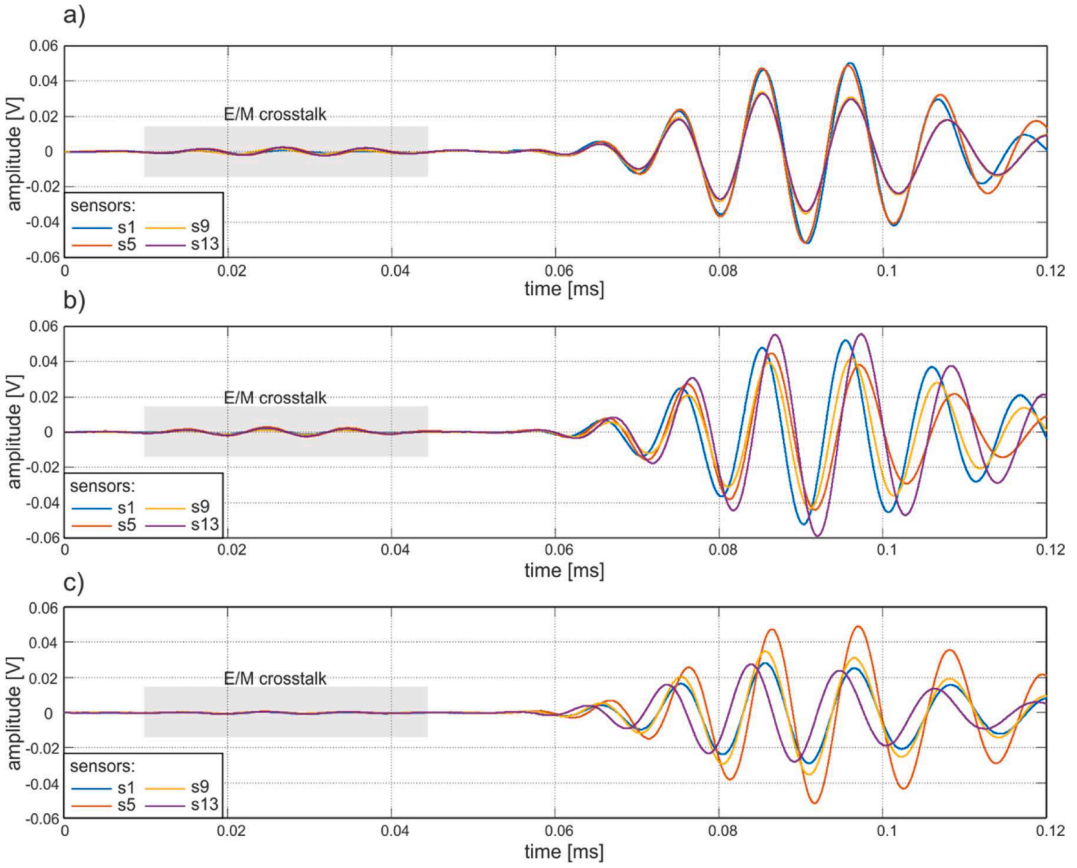

Fig. 24. Exemplary experimental wave propagation signals obtained for variable DoD: a) DoD = 0 %, b) DoD = 10 % and DoD = 20 % for a frequency of 100 kHz.

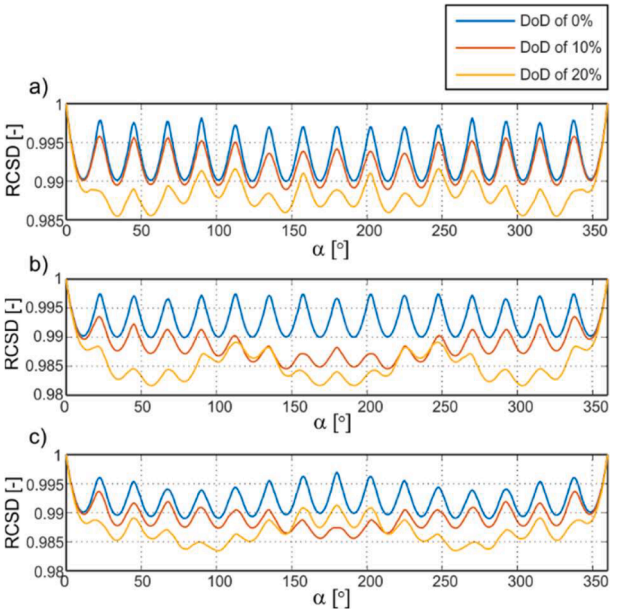

Fig. 25. RCSD functions determined for plates varying in DoD: a) RCSD determined for excitation frequency of 50 kHz, b) 100 kHz and c) 150 kHz.

ultrasonic gauge measurements revealed variability in thickness. This variability could stem from the initial preparation process preceding the experimental tests, during which the plate underwent special cleaning and polishing, potentially introducing thickness variations through mechanical surface treatment. Consequently, the ToF measured at different locations may exhibit slight discrepancies. All these factors might influence both ToF and the signal amplitude. As presented in [35], the exact geometry (not only thickness distribution in the statistical sense) significantly impacts amplitude variability, which is also visible for registered signals.

The differences between the signals become more pronounced as the DoD increases. The incident waves undergo noticeable shifts relative to each other, signifying the asymmetry inherent in the wave propagation field. This asymmetry aligns with both numerical simulations and theoretical predictions. Analogous to prior procedures, the experimental signals underwent processing to ascertain the ToF and to reconstruct the wavefronts In the subsequent phase, the acquired wavefronts were employed to determine the RCSD and BCSD functions, as illustrated in Fig. 25 and Fig. 26, respectively. A discernible correlation exists between the values of these functions and the DoD in relation to symmetry degrees. Generally, an inverse relationship is observed, wherein the symmetry level diminishes concomitant with escalating degradation levels. This trend persists irrespective of the excitation frequency, whether at 50 kHz, 100 kHz, or 150 kHz. Notably, at the lowest frequency of 50 kHz, all peaks of RCSD and BCSD functions exhibit a reduction as the DoD increases.

Conversely, for higher frequencies (100 kHz and 150 kHz), specific rotational angles (α) can be identified wherein central symmetry degrees are elevated for lower DoDs. For instance, this phenomenon is evident in Fig. 25b for α values ranging from 120° to 130° and in Fig. 25c for α values spanning from 160° to 180°. The possible explanation is that the A0 mode exhibits the highest dispersion for the low frequencies and, thus, is the most sensitive to thickness variations.

The quantity of peaks in all graphed functions corresponds precisely to the number of attached sensors. Nevertheless, none of the ascertained RCSD and BCSD values attained the theoretical maximum value of 1. The physical meaning of this is that it was impossible to distinguish any symmetry axis for the experimentally determined wavefront shape, even in the undamaged plate. The deviation from the maximum theoretical value can be treated as uncertainty caused by imperfect transducers attachment or errors in ToF estimation. Nevertheless, the experimental results (Fig. 25 and Fig. 26) demonstrated more significant differences for varying DoD than analogous numerical results (Fig. 18 and Fig. 19). The reason for a more clearly observed decreasing trend in the case of experimental results is associated with the experimental corrosion process. The corrosion degradation affects on both surface morphology, as well as the average thickness of the plate. With increasing DoD, the plate surface also changes. Thus, the functions given in Fig. 25 and Fig. 26 demonstrate the cumulative effect of DoD and surface irregularities on the wavefront propagation. In the case of numerical simulations, the DoD was variable, but the standard deviation of the thickness distribution was the same for plate B# and C#.

Fig. 27 and Fig. 28 present the maximum and minimum values of symmetry degrees extracted from experimental and numerical RCSD and BCSD functions, incorporating horizontal grey and green lines A and B denoting the theoretical extremes established for a sensor network comprised of 16 sensors. Solid lines represent experimental values, while dashed lines represent numerical results. Consistently, irrespective of the nature of symmetry (rotational or bilateral) and the specific symmetry degree (minimum or maximum) under consideration, a distinctly discernible diminishing trend has been observed with the progression of corrosion-induced damage. Moreover, the slopes of the particular lines are comparable for numerical and experimental cases. The main difference between the experimental and numerical results is their absolute values: the symmetry degrees obtained numerically are higher, which is associated

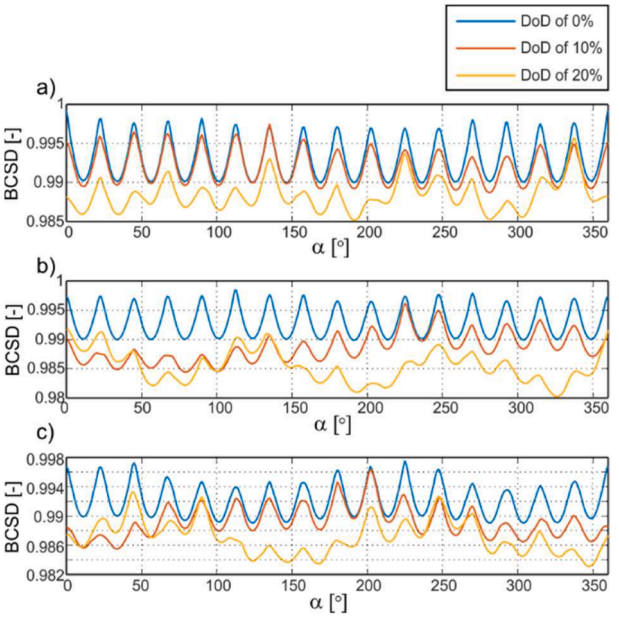

Fig. 26. BCSD functions determined for plates varying in DoD: a) BCSD determined for excitation frequency of 50 kHz, b) 100 kHz and c) 150 kHz.

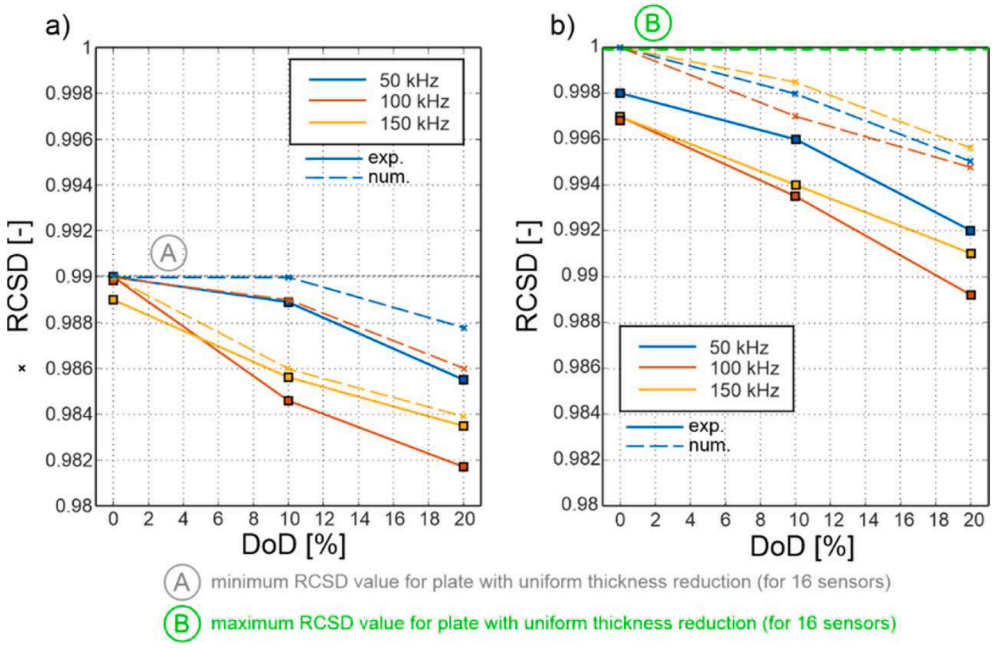

Fig. 27. Minimum and maximal values of RCSD functions determined for plates varying in DoD: a) minimum values of RCSD and b) maximum values of RCSD for variable frequencies.

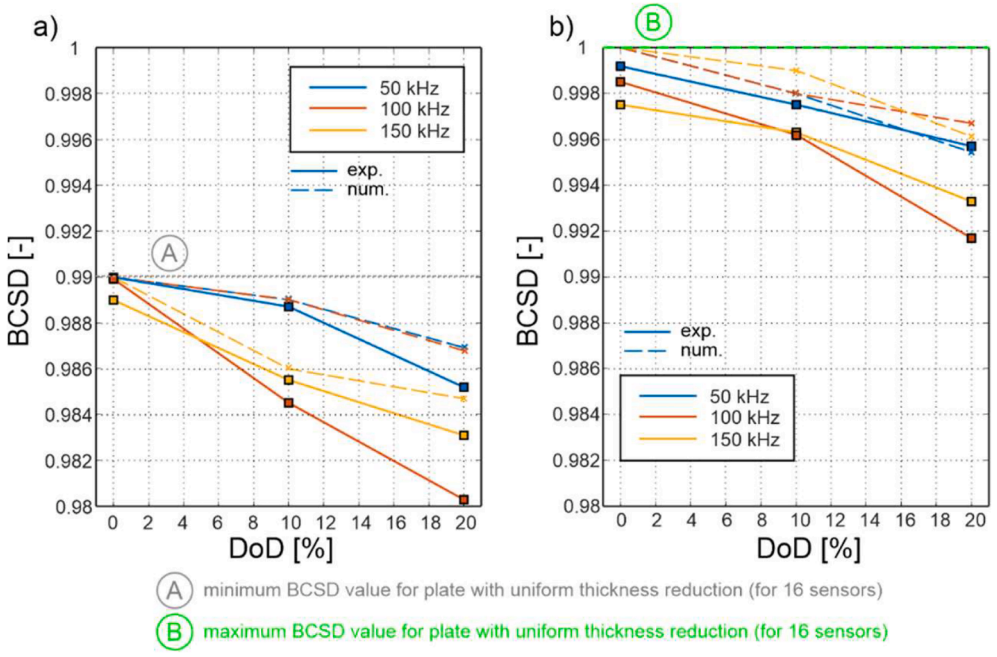

Fig. 28. Minimal and maximal values of BCSD functions determined for plates varying in DoD: a) minimum values of BCSD and b) maximum values of BCSD for variable frequencies.

with the homogeneity of the material and precise selection of the sensor node in the numerical model, which was more challenging to achieve in experimental tests. Despite that, the numerical and experimental results coincide well. The employed frequencies varied in dispersion level and exhibited different sensitivities to thickness variations, but a decreasing trend was noted in each case.

Despite a clear decreasing trend with increasing DoD obtained for both experimental and numerical results, we can also observe the differences between the obtained results. In Fig. 27b, the highest symmetry degrees were noted for 150 kHz, then for 50 kHz and next for 100 kHz. The order of curves differs for experimental results when the highest RCSD values were obtained for 50 kHz, then for 150

kHz and 100 kHz. Such shift is also observed in other cases: experimentally, the highest symmetry degrees were noted for 50 kHz in all considered cases i.e. for this frequency the wavefront was “most symmetric”. A possible explanation might be the measurement uncertainty. The wave packet for 50 kHz has the most significant time duration and was not characterized by the highest SNR in our study. Due to the relatively small monitored area, long time duration of the wave packet and the signal noise, for 50 kHz it was more difficult to observe changes in ToF, which determined the decrease in the degree of symmetry. However, the influence of the excitation frequency and associated effects i.e., SNR on wavefront symmetry assessment was not considered in detail and requires further investigations, which would allow for formulations of the guidelines for mode selection.

6. Discussion and conclusions

This section summarizes the results and indicates the limitations and necessary future studies on the developed approach. The presented investigation was focused on the impact of Degrees of Degradation (DoD), standard deviation of thickness distribution, and excitation frequency on the symmetry degrees of wavefronts. Several noteworthy conclusions can be drawn from the findings:

- The experimental tests indicated that corrosion damage leads to nonuniform degradation, and therefore wave propagation velocity depending on plate thickness may be characterized by significant variation. Because the dispersion relations are usually nonlinear, the assumption that wave velocity measured on a certain distance can be used for assessing the average thickness can be associated with some inaccuracies.
- In this study, three different frequencies were initially selected based on the SNR ratio and next were used for symmetry degree determination. They varied in the dispersion level and, therefore, should exhibit different sensitivities to thickness variations. Meanwhile, regardless of the dispersion level, the decreasing trend of symmetry degree with increasing DoD was noted in all cases. The main difference between particular frequencies was in symmetry functions. For the lowest and most dispersive frequency (50 kHz), all peaks of RCSD and BCSD functions exhibit a reduction as the DoD increases.
- Conversely, for higher frequencies (100 kHz and 150 kHz), specific rotational angles (α) could be identified wherein values of RCSD and BCSD functions were elevated for lower DoDs. On the other hand, when the extreme symmetry degrees have been extracted from symmetry functions, the higher frequencies (100 and 150 kHz) exhibit more unambiguous trends, with extreme symmetry degrees consistently increasing with DoD and standard deviation. At lower frequencies (50 kHz), especially for significant DoD, results are less unequivocal, and disruptions in functional trends are observed for the most severely corroded plates. The longer wavelengths, associated with lower frequencies, display a degree of insensitivity to minor thickness changes and surface roughness. This characteristic suggests the potential for more reliable and unambiguous results in specific scenarios. However, the influence of the excitation frequency on wavefront symmetry assessment was not considered here in detail and requires further investigations, which would allow for formulations of the guidelines for mode selection.
- The research establishes a substantial influence of DoD on both BCSD and RCSD functions. Notably, higher DoD values consistently lead to decreased symmetry degrees, emphasizing the sensitivity of wavefront symmetry to structural degradation. The main reason for variable propagation velocity in different directions is the complex geometry of the degraded specimen. Therefore, the effect of velocity changes is more visible for specimens with higher DoD. On the other hand, the symmetry degrees are completely independent of the exact ToFs. They depend only on the difference in ToFs noted for the particular sensors. It can be considered as an advantage because it excludes the influence of systematic errors in ToF estimation. Moreover, detailed knowledge about dispersion curves (and in consequence, about material properties) is not required. However, considering only differences in ToF without considering their exact values means that if the degradation were uniform, the presented approach would be ineffective as the propagation wavefront would be symmetric. This is one of the limitations of the proposed approach. One possible solution to eliminate or reduce the possibility of incorrect corrosion assessment is to develop a combined approach exploiting the currently developed ToF-based methods for average thickness determination and symmetry-based methods. The problem of combining these two approaches to elevate the reliability of corrosion assessment should be considered in the following steps.
  - The study underscores the indispensable influence of the standard deviation of thickness distribution, representing surface roughness, on wavefront symmetry. Increased roughness correlates with more significant variability in wave propagation velocity and lower symmetry degree values. The main advantage of this is the possibility of even an insignificant DoD decrease if it is associated with a surface roughness increase. However, despite the overall trends, disruptions in functional courses are observed (i.e., symmetry degrees increased despite increasing DoD), particularly for severely corroded plates. This means that the significant roughness of the plate surface may affect the estimation accuracy of the average thickness reduction. As mentioned, the combined approach considering the exact values of the ToF and its relative changes due to degradation might be the solution for this limitation. The more profound insight into the physical aspects of the wave propagation phenomena in irregular plates is crucial for further developing these methods.
  - Despite promising results, the presented method has some limitations. First of all, it is sensitive to measurement uncertainty, and moreover, the influence of the measurement uncertainty is not always the same, i.e., the imperfect attachment of two sensors placed next to each other has a more significant impact on the wavefront symmetry degree, than the imperfect attachment of the two sensors located 180 degrees apart. Therefore, assessing the influence of uncertainty might be more difficult in the case of the proposed method. The second limitation is the need for a specific sensor network arrangement. The paper presents the initial results and demonstrates the possibility of using wavefront symmetry in corrosion assessment. However, the need to use a circular sensor array may be very challenging in the case of real structures, especially in the extended sensor network, which facilitates wavefront reconstruction and may positively influence the measurement accuracy. The presented method is also

ineffective if the corrosion does not impact the surface roughness. We can still assess the thickness reduction using averaged ToF, but the symmetry degrees are sensitive only to irregularities.

Moreover, the symmetry degree varies only in the limited range, even for the significant thickness reduction. This means that the notable corrosion degradation may cause an insignificant reduction in symmetry degree, which entails problems with the inverse problem solution. The limitations mentioned above are also the possible directions for further investigation.

The study underscores the multifaceted interplay of degradation, surface roughness, and excitation frequency in shaping wavefront symmetry, offering valuable insights for structural health monitoring and nondestructive evaluation applications. Despite that, there are several areas which must be considered in the future studies:

- Assessment of the influence of the sensor network's extent and the distance from the actuator: the longer the distance from the actuator, the larger the monitored area. On the other hand, the lower resolution of the monitoring system and the lower accuracy of the corrosion degradation we have;
- Uncertainty analysis: The second important aspect crucial for practical application, which was not considered here, is the assessment of the proposed method's reliability, including uncertainty analysis. Perfect repeatability is usually not possible to obtain and in this study, the errors in ToF due to uncertainty of transducers attachment reached 1.5 %. Despite the inaccuracies, a decreasing trend in symmetry degrees with the progress of corrosion degradation was observed for the plates considered. However, uncertainty analysis is crucial for developing the proposed approach, especially in solving inverse problems aimed at estimating the DoD and surface roughness based on the wavefront symmetry degrees.
- Possibility of corrosion detection in an early stage of its development: corrosion detection is crucial, especially in its early development stage. It allows for the repair or for the further monitoring of the damaged areas. The results presented in the paper indicate that the proposed methodology can be effective in the case of relatively low DoD (up to 20 %). However, it would be beneficial to develop procedures that allow for the distinguishing and evaluating of both DoD and the surface roughness effect on the wavefield symmetry, especially if their values are relatively low and the influence of the inaccuracies is significant. The target effect would be determining the probability of corrosion detection for the variable parameters describing thickness and plate surface.

Ethical statement

The authors state that the research was conducted according to ethical standards.

CRediT authorship contribution statement

Beata Zima: Writing – original draft, Visualization, Software, Resources, Project administration, Methodology, Investigation, Funding acquisition, Formal analysis, Conceptualization. **Jochen Moll:** Writing – original draft, Conceptualization.

Declaration of competing interest

The authors declare that they have no known competing financial interests or personal relationships that could have appeared to influence the work reported in this paper.

Data availability

Data will be made available on request.

Acknowledgment

The research was carried out within project No. 2021/43/D/ST8/00786, financed by the National Science Centre, Poland. Abaqus calculations were carried out at the Academic Computer Centre in Gdańsk.

References

[1] F. Qiu, H. Wang, H. Qian, H. Hu, X. Jin, F. Fan, Evaluation of compressive properties of the ship plate after seawater corrosion based on 3D evolution prediction, Ocean Eng. 266 (2022) 112561.
[2] S. Mahadevan, P. Shi, Corrosion fatigue reliability of aging aircraft structures, Prog. Struct. Eng. Mater. 3 (2) (2001) 188–197.
[3] J. Bhandari, F. Khan, R. Abbassi, V. Garaniya, R. Ojeda, Modelling of pitting corrosion in marine and offshore steel structures – A technical review, J. Loss Prev. Process Ind. 37 (2015) 39–62.
[4] International Association of Classification Societies Recommendation 87. Guidelines for Coating Maintenance & Repairs for Ballast Tanks and Combined Cargo/ ballast Tanks on Oil Tankers (2015).
[5] Seah K. H., Karim M. F., Ong L. C., Chiam T. M., Rapid corrosion detection using 94 GHz millimeter wave technology. 2012 IEEE International Instrumentation and Measurement Technology Conference Proceedings, Graz, Austria (2012) 473-476.
[6] Eddazi A, Belattar S. Nondestructive Testing Evaluation of Aircraft Fuselage Corrosion by Infrared Thermography and Finite Element Method. International Conference on Computer Graphics Imaging and Visualization (2017) 56-61.

[7] Z. Su, L. Ye, Y. Lu, Guided Lamb waves for identification of damage in composites: A review, J. Sound Vib. 295 (2006) 753–780.
[8] A. Farhidzadeh, S. Salamone, Reference-free corrosion damage diagnosis in steel strands using guided ultrasonic waves, Ultrasonics 57 (2015) 198–208.
[9] B. Zima, K. Woloszyk, Y. Garbatov, Experimental and numerical identification of corrosion degradation of aging structural components, Ocean Eng. 258 (2022) 111739.
[10] H. Sun, W. Shao, J. Song, X. Yang, Y. Wang, X. Qing, Corrosion quantification of plate-type structures using Lamb wavefield and monogenic signal processing, Ultrasonics 130 (2023) 106935.
[11] J. Hua, X. Cao, Y. Yi, J. Lin, Time-frequency damage index of Broadband Lamb wave for corrosion inspection, J. Sound Vib. 464 (2020) 114985.
[12] X. Ding, C. Xu, M. Deng, Y. Zhao, X. Bi, N. Hu, Experimental investigation of the surface corrosion damage in plates based on nonlinear Lamb wave methods, NDT&E International 121 (2021) 102466.
[13] C. Nicard, M. Farin, E. Moulin, D. Balloy, I. Serre, Monitoring of generalized corrosion: Ultrasonic coda wave interferometry technique applied to steel corrosion in aqueous NaCl solutions, Mater. Chem. Phys. 305 (2023) 127908.
[14] A. Gajdacsi, F. Cegla, The effect of corrosion induced surface morphology changes on ultrasonically monitored corrosion rates, Smart Mater. Struct. 25 (2016) 15010.
[15] R. Howard, F. Cegla, Detectability of corrosion damage with circumferential guided waves in reflection and transmission, NDT&E International 91 (2017) 108–119.
[16] R. Howard, F. Cegla, On the probability of detecting wall thickness defects with dispersive circumferential guided waves, NDT&E International 86 (2017) 73–82.
[17] F. Zou, F. Cegla, High-accuracy ultrasonic corrosion rate monitoring, Corrosion 74 (3) (2018) 372–382.
[18] Howard R., Cegla F. The effects of pits of different sizes on ultrasonic shear wave signals. 44th Annual review of progress in quantitative nondestructive evaluation 1949(1) (2018) 050002.
[19] F.L. Di Scalea, S. Salamone, Temperature effects in ultrasonic Lamb wave structural health monitoring systems, J. Acoust. Soc. Am. 124 (2008) 161.
[20] M. Toa, A. Whitehead, Ultrasonic sensing, Ultrasonics 3 (2020) 217.
[21] L.W. Schmerr Jr., Fundamentals of Ultrasonic Nondestructive Evaluation: A modeling Approach, 2nd ed., Springer International Publishing, Cham, Switzerland, 2016.
[22] P. Khalili, P. Cawley, The choice of ultrasonic inspection method for the detection of corrosion at inaccessible locations, NDT E International 99 (2018) 80–92.
[23] Rathod V., Roy Mahapatra D. Ultrasonic Lamb wave based monitoring of corrosion type of damage in the plate using a circular array of piezoelectric transducers, NDT&E International 44 (2011) 628-636.
[24] B. Zima, E. Roch, J. Moll, Nondestructive corrosion degradation assessment based on asymmetry of guided wave propagation field, Ultrasonics 138 (2024) 107243.
[25] B. Zima, J. Moll, Numerical and experimental investigation of guided ultrasonic wave propagation in nonuniform plates with structural phase variations, Ultrasonics 128 (2023) 106885, https://doi.org/10.1016/j.ultras.2022.106885.
[26] B. Zima, J. Moll, Theoretical and experimental analysis of guided wave propagation in plate-like structures with sinusoidal thickness variations, Archiv. Civ. Mech. Eng. 23 (2023) 34.
[27] Y. Cho, Estimation of ultrasonic guided wave mode conversion in a plate with thickness variation, IEEE Trans. Ultrason. Ferromagnet. 47 (3) (2000) 591.
[28] M.V. Predoi, M.E.C. El-Kettani, Z. Hamitouche, C.C. Petre, Guided waves in plates with linear variation of thickness, J. Acoust. Soc. Am. 123 (5) (2008) 3834.
[29] P. Marical, M.E.C. El-Kettani, M.V. Predoi, Guided waves in elastic plates with Gaussian section variation Experimental and numerical results, Ultrasonics 47 (2007) 1–9.
[30] Z. Hu, Z. An, Y. Kong, G. Lian, X. Wang, The nonlinear S0 Lamb mode in a plate with a linearly-varying thickness, Ultrasonics 94 (2019) 102–108.
[31] J. Moll, T. Wandowski, P. Malinowski, M. Radzienski, S. Opoka, W. Ostachowicz, Experimental analysis and prediction of antisymmetric wave motion in a tapered anisotropic waveguide, J. Acoust. Soc. Am. 138 (2015) 299–306.
[32] Lamb H. On waves in elastic plate. Proceedings of the Royal Society of London. Series A. London 93 (1917) 114–128.
[33] L. De Marchi, A. Marzani, N. Speciale, E. Viola, Prediction of pulse dispersion in tapered waveguides, NDT and E Int. 43 (3) (2010) 265–271.
[34] J. Moll, T. Wandowski, P. Malinowski, M. Radzienski, S. Opoka, W. Ostachowicz, Experimental analysis and prediction of antisymmetric wave motion in a tapered anisotropic waveguide, J. Acoust. Soc. Am. 138 (1) (2015) 299–306.
[35] B. Zima, Determination of stepped plate thickness distribution using guided waves and compressed sensing approach, Measurement 196 (2022) 111221.
[36] R. Kiciński, A. Kubit, Small Caliber Bulletproof Test of Warships' Hulls, Materials (Basel) 13 (17) (2020) 3848.
[37] L.R. Rabiner, B. Gold, Theory and application of digital signal processing, Prentice-Hall, 1975.
[38] H. Gravenkamp, Efficient simulation of elastic guided waves interacting with notches, adhesive joints, delaminations and inclined edges in plate structures, Ultrasonics 82 (2018) 101–113.
[39] X. Liu, W. Zhang, X. Gu, Z. Ye, Probability distribution model of stress impact factor for corrosion pits of high-strength prestressing wires, Eng. Struct. 230 (2021) 111686.
[40] Y. Garbatov, C. Guedes Soares, G. Wang, Nonlinear time dependent corrosion wastage of deck plates of ballast and cargo tanks of tankers, J. Offshore Mech. Art. Eng. 129 (2007) 48–55.
[41] Contantine P, Wang Q. Random field simulation. MATLAB Central File Exchange. Retrieved June 28, 2023.
[42] P. Domzalicki, I. Skalski, S.C. Guedes, Large Scale Corrosion Tests, in: P.K. Das (Ed.), Analysis and Design of Marine Structures, Taylor & Francis Group, 2009, pp. 193–198.
[43] B. Nie, S. Xu, J. Yu, H. Zhang, Experimental investigation of mechanical properties of corroded cold-formed steels, J. Constr. Steel Res. 162 (2019) 105706.
[44] Q. Guo, F. Guo, J. Shao, Irregular shape symmetry analysis: Theory and application to quantitative galaxy classification, IEEE Trans. Pattern Anal. Mach. Intell. 32 (10) (2010) 1730–1743.